Advances in Numerical Modeling of Astrophysical and Space Plasmas

Dedicated to the memories of Hannes Alfvén and Oscar Buneman; Founders of the Subject.

Anthony L. Peratt *
Los Alamos National Laboratory
Los Alamos, New Mexico, USA

Abstract. Plasma science is rich in distinguishable scales ranging from the atomic to the galactic to the meta-galactic, i.e., the *mesoscale.* Thus plasma science has an important contribution to make in understanding the connection between microscopic and macroscopic phenomena. Plasma is a system composed of a large number of particles which interact primarily, but not exclusively, through the electromagnetic field. The problem of understanding the linkages and couplings in multi-scale processes is a frontier problem of modern science involving fields as diverse as plasma phenomena in the laboratory to galactic dynamics.

Unlike the first three states of matter, plasma, often called the fourth state of matter, involves the mesoscale and its interdisciplinary founding have drawn upon various subfields of physics including engineering, astronomy, and chemistry. Basic plasma research is now posed to provide, with major developments in instrumentation and large-scale computational resources, fundamental insights into the properties of matter on scales ranging from the atomic to the galactic. In all cases, these are treated as mesoscale systems. Thus, basic plasma research, when applied to the study of astrophysical and space plasmas, recognizes that the behavior of the near-earth plasma environment may depend to some extent on the behavior of the stellar plasma, that may in turn be governed by galactic plasmas. However, unlike laboratory plasmas, astrophysical plasmas will forever be inaccessible to in situ observation. The inability to test concepts and theories of large-scale plasmas leaves only virtual testing as a means to understand the universe. Advances in in computer technology and the capability of performing physics first principles, fully three-dimensional, particle–in–cell simulations, are making virtual testing a viable alternative to verify our predictions about the far universe.

The first part of this paper explores the dynamical and fluid properties of the plasma state, plasma kinetics, and the radiation emitted from plasmas. The second part of this paper outlines the formulation for the particle-in-cell simulation of astrophysical plasmas and advances in simulational techniques and algorithms, as-well-as the advances that may be expected as the computational resource grows to petaflop speed/memory capabilities.

Key words: Numerical Simulation, Astrophysical Plasmas, Space Plasmas, Plasma Universe, Electric Space

* Scientific Advisor, Office of Research and Development, United States Department of Energy, Washington D.C.

Astrophysics and Space Science **242**: 93–163, 1997.

1. "In-Situ" Observation of Astrophysical and Space Plasmas via Computer Simulation

While it is thinkable that our ability to make in situ measurements can perhaps be extended to the nearest stars, most of the universe beyond a few parsecs will be beyond the reach of our spacecraft forever.

From one's unaided view of the clear night sky, it is tantalizing to believe that the physics of the universe can be unfolded from the observable stars, which may be up to kiloparsecs away, or from the fuzzy "nebula" such as the galaxy M31, nearly a megaparsec away. Our experience in unfolding energetic events in our own solar system suggests otherwise.

The inability to make in situ observations places a severe constraint on our ability to understand the universe, which is to say, astrophysical and space plasmas, even when the full electromagnetic spectrum is available to us. Only in the last $2\frac{1}{2}$ decades, after satellites monitored our near-earth environment and spacecraft discovered and probed the plasma magnetospheres of the planets, could we begin to get a true picture of the highly-energetic processes occurring everywhere in the solar system. These plasma processes included large-scale magnetic-field-aligned currents and electric fields and their role in the transport of energy over large distances. The magnetospheres of the planets are invisible in the visual octave (400-800 nm) and from earth cannot even be positively identified in the X ray and gamma ray regions, which cover 10 times as many octaves and have more than 1,000 times the bandwidth as the visual octave. Only in the low frequency radio region is there a hint of the presence of quasi-static electric fields which accelerate charged particles in the magnetospheres of the planets.

As the properties of plasma immediately beyond the range of spacecraft are thought not to change, it must be expected that plasma sources of energy and the transport of that energy via field-aligned currents exist at even larger scales than that found in the solar system. How then are we to identify these mechanisms in the distant universe?

The advent of particle-in-cell (PIC) simulation of cosmic plasmas on large computer systems ushered in an era whereby in situ observation in distant or inaccessible plasma regions is possible. While the first simulations were simple, with many physics issues limited by constraints in computer speed and memory, it is now possible to study the full three-dimensional, fully-electromagnetic evolution of magnetized plasma over a very large range of sizes. In addition, PIC simulations have matured enough to contain Monte Carlo collisional scattering and energy loss treatments, conducting sheets or surfaces, dielectric regions, space-charge-limited emission from surfaces and regions, and electro-

magnetic wave propagation. Since a simulation involves the motion of charge or mass particles according to electromagnetic or gravitational forces, all in situ information is available to the simulationist.

If the simulation correctly models the cosmic plasma object under study, replication of observations over the entire electromagnetic spectrum should be expected, to the extent that the model contains sufficient temporal and spatial resolution.

However, before the simulationist can model a particular problem of astrophysical or space plasma interest, fundamental knowledge is required about the nature of the plasma state under study, its characteristic properties and behavior, its evolution, but perhaps most importantly, its mesoscale physics especially in regards to plasmas of larger dimensions which are most probably the source of energy of the observed radiation.

2. The Plasma State

2.1. Plasma

Plasma consists of electrically charged particles that respond collectively to electromagnetic forces. The charged particles are usually clouds or beams of electrons or ions, or a mixture of electrons and ions, but also can be charged grains or dust particles. Cosmic plasma is also at temperatures comparable to or higher than that in the interior of stars. At these temperatures, only the constituent building blocks of light atoms exist: positively charged bare nuclei and negatively charged free electrons. The name plasma is also properly applied to ionized gases at lower temperatures where a considerable fraction of neutral atoms or molecules are present.

While all matter is subject to gravitational forces, the positively charged nuclei, or ions, and the negatively charged electrons of plasmas react strongly to electromagnetic forces, as formulated by Oliver Heaviside (1850-1925),[1] but now called Maxwell's Equations, after James Clerk Maxwell (1831-1879),[2]

$$\frac{\partial \mathbf{B}}{\partial t} = -\nabla \times \mathbf{E} \tag{1}$$

[1] Oliver Heaviside was the first to reduce Maxwell's 20 equations in 20 variables to the two equations 1 and 2 in vector field notation. For some years Eqs. 1- 4 were known as the Hertz-Heaviside Equations, and later A. Einstein called them the Maxwell-Hertz Equations. Today, only Maxwell's name is mentioned [Nahin 1988].

[2] These are "rewritten" in update form ideal for programming. This also emphasizes the causality correctly: curl **E** is the cause of changes in **B**, curl **H** is the cause of changes in **D**.

$$\frac{\partial \mathbf{D}}{\partial t} = \nabla \times \mathbf{H} - \mathbf{j} \tag{2}$$

$$\nabla \cdot \mathbf{D} = \rho \tag{3}$$

$$\nabla \cdot \mathbf{B} = \mathbf{0} \tag{4}$$

and the equation of motion due to Hendrik Antoon Lorentz (1853-1928),

$$\frac{d}{dt}(m\mathbf{v}) = q(\mathbf{E} + v \times \mathbf{B}); \quad \frac{d\mathbf{r}}{dt} = \mathbf{v}; \tag{5}$$

The quantities $\mathbf{D} = \epsilon\mathbf{E}$ and $\mathbf{B} = \mu\mathbf{H}$ are the constitutive relations between the electric field $\mathbf{E}$ and the displacement $\mathbf{D}$ and the magnetic induction $\mathbf{B}$ and magnetic intensity $\mathbf{H}$, μ and ϵ are the permeability and permittivity of the medium, respectively, and ρ and $\mathbf{j}$ are the charge and current densities, respectively.[3] The mass and charge of the particle obeying the force law (Eq. 5) are m and q, respectively.

Because of their strong interaction with electromagnetism, plasmas display a complexity in structure and motion that far exceeds that found in matter in the gaseous, liquid, or solid states. For this reason, plasmas, especially their electrodynamic properties, are far from understood. Irving Langmuir; (1881-1957), the electrical engineer and Nobel chemist, coined the term plasma in 1923, probably borrowing the term from medical science to describe the collective motions that gave an almost lifelike behavior to the ion and electron regions with which he experimented. Langmuir was also the first to note the separation of plasma into cell-like regions separated by charged particle sheaths. Today, this cellular structure is observed wherever plasmas with different densities, temperatures, magnetic field strengths, chemical constituencies, or matter–antimatter plasmas come in contact.

Plasmas need not be neutral (i.e., balanced in number densities of electrons and ions). Indeed, the study of pure electron plasmas and even positron plasmas, as well as the electric fields that form when electrons and ions separate, are among the most interesting topics in plasma research today. In addition to cellular morphology, plasmas often display a filamentary structure. This structure derives from the fact that plasma, because of its free electrons, is a good conductor of electricity, far exceeding the conducting properties of metals such as copper or gold. Wherever charged particles flow in a neutralizing medium, such as free electrons in a background of ions, the charged particle flow or current produces a ring of magnetic field around the current, pinching the current into filamentary strands of conducting currents.

[3] In free space $\epsilon = \epsilon_0 = 8.8542 \sim 10^{-12}$ farad m^{-1} and $\mu = \mu_0 = 4\pi \sim 10^{-7}$ henry m^{-1}.

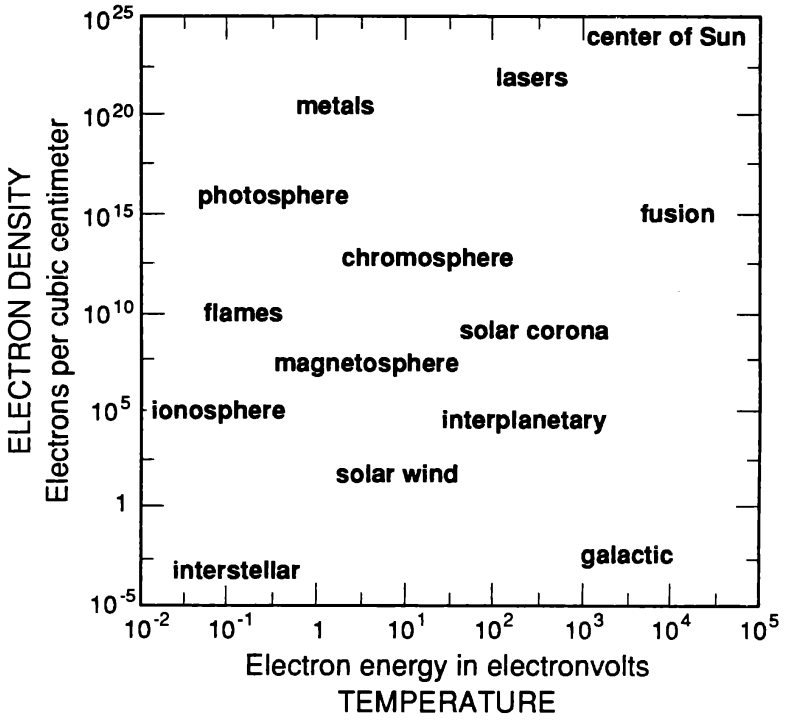

Figure 1. The remarkable range of temperatures and densities of plasmas is illustrated by this chart. In comparison, solids, liquids, and gases exist over a very small range of temperatures and pressures. In "solid" metals, the electrons that carry an electric current exist as a plasma within the more rigid crystal structure.

Matter in the plasma state can range in temperature from hundreds of thousands of electronvolts (1 eV = 11,605 degrees absolute) to just one-hundredth of an electronvolt. In density, plasmas may be tenuous, with just a few electrons present in a million cubic centimeters, or they may be dense, with more than 10^{20} electrons packed per cubic centimeter (Figure 1). Nearly all the matter in the universe exists in the plasma state, occurring predominantly in this form in the Sun and stars and in interstellar space. Auroras, lightning, and welding arcs are also plasmas. Plasmas exist in neon and fluorescent tubes, in the sea of electrons that moves freely within energy bands in the crystalline structure of metallic solids, and in many other objects.

Above all, plasmas are prodigious producers of electromagnetic radiation; from the highest energy gamma rays, to microwaves, to extremely low frequencies which, in our time frame may be considered to be practically dc.

2.2. The Physical Sizes and Characteristics of Plasmas in the Universe

Volume-wise, 99.999% of all the observable matter in the universe exists in the plasma state.

2.2.1. *Plasmas on Earth*

On the earth, plasmas are found with dimensions of microns to meters, that is, sizes spanning six orders of magnitude. The magnetic fields associated with these plasmas range from about 0.5 gauss (the earth's ambient field) to megagauss field strengths. Plasma lifetimes on earth span 12 to 19 orders of magnitude: Laser produced plasmas have properties measurable in picoseconds, pulsed power plasmas have nanosecond to microsecond lifetimes, and magnetically confined fusion oriented plasmas persist for appreciable fractions of a second. Quiescent plasma sources, including fluorescent light sources, continuously produce plasmas whose lifetimes may be measured in hours, weeks, or years, depending on the cleanliness of the ionization system or the integrity of the cathode and anode discharge surfaces.

Lightning is a natural plasma resulting from electrical discharges in the earth's lower troposphere. Such flashes are usually associated with cumulonimbus clouds but also occur in snow and dust storms, tornadoes, active volcanos, nuclear explosions, and ground fracturing. The maximum time duration of a lightning flash is about 2 s in which peak currents as high as 200 kA can occur. The conversion from air molecules to a singly ionized plasma occurs in a few microseconds, with hundreds of megajoules of energy dissipated and plasma temperatures reaching 3 eV. The discharge channel avalanches at about one-tenth the speed of light, and the high current carrying core expands to a diameter of a few centimeters. The total length of the discharge is typically 2-3 km, although cloud-to-cloud discharges can be appreciably longer. Lightning has been observed on Jupiter, Saturn, Uranus, and Venus. The energy released in a single flash on earth, Venus, and Jupiter is typically 6×10^8 J, 2×10^{10} J, and 2.5×10^{12} J, respectively.

Nuclear driven atmospheric plasmas were a notable exception to the generally short-lived energetic plasmas on earth. For example, the 1.4 megaton (5.9×10^{15} J) Starfish detonation, 400 km above Johnston Island, on July 9, 1962, generated plasma from which artificial Van Allen belts of electrons circulating the earth were created. These electrons, bound at about 1.2 earth-radii in a 0.175 G field, produced synchrotron radiation whose decay constant exceeded 100 days.

2.2.2. *Near-Earth Plasmas*

The earth's ionosphere and magnetosphere constitute a cosmic plasma system that is readily available for extensive and detailed in situ observation and even active experimentation. Its usefulness as a source of understanding of cosmic plasmas is enhanced by the fact that it contains a rich variety of plasma populations with densities ranging from more than 10^6 cm^{-3} to less than 10^{-2} cm^{-3}, and temperatures from about 0.1 eV to more than 10 keV.

The earth's magnetosphere is that region of space defined by the interaction of the solar wind with the earth's dipole-like magnetic field. It extends from approximately 100 km above the earth's surface, where the proton neutral atom collision frequency is equal to the proton gyrofrequency, to about ten earth radii ($\sim$ 63,800 km) in the sunward direction and to several hundred earth radii in the anti-sunward direction.

First detected by radio waves and then by radar, the ionosphere is a layered plasma region closest to the surface of the earth whose properties change continuously during a full day. First to be identified was a layer of molecular ionization, called the E layer. This region extends over a height range of 90-140 km and may have a nominal density of 10^5 cm^{-3} during periods of low solar activity. A D region underlies this with a nominal daytime density of 10^3 cm^{-3}. Overlaying the E region is the F layer of ionization, the major layer of the ionosphere, starting at about 140 km. In the height range 100-150 km, strong electric currents are generated by a process analogous to that of a conventional electric generator, or dynamo. The region, in consequence, is often termed the dynamo region and may have densities of 10^6 cm^{-3}. The F layer may extend 1,000 km in altitude where it eventually merges with the plasmas of the magnetopause and solar wind.

The interaction of the supersonic solar wind with the intrinsic dipole magnetic field of the earth forms the magnetosphere whose boundary, called the magnetopause, separates interplanetary and geophysical magnetic fields and plasma environments. Upstream of the magnetopause a collisionless bow shock is formed in the solar wind-magnetosphere interaction process. At the bow shock the solar wind becomes thermalized and subsonic and continues its flow around the magnetosphere as magnetosheath plasma, ultimately rejoining the undisturbed solar wind.

In the anti-solar direction, observations show that the earth's magnetic field is stretched out in an elongated geomagnetic tail to distances of several hundred earth radii. The field lines of the geomagnetic tail intersect the earth at high latitudes ($\approx 60° - 75°$) in both the northern and southern hemisphere (polar horns), near the geomagnetic

poles. Topologically, the geomagnetic tail roughly consists of oppositely directed field lines separated by a "neutral" sheet of nearly zero magnetic field. Surrounding the neutral sheet is a plasma of "hot" particles having a temperature of 1-10 keV, density of $\approx$0.01-1 cm^{-3}, and a bulk flow velocity of a few tens to a few hundreds of km s^{-1}.

Deep within the magnetosphere is the plasmasphere, a population of cold ($\leq$ 1 eV) ionospheric ions and electrons corotating with the earth.

2.2.3. *Plasmas in the Solar System*

The space environment around the various planetary satellites and rings in the solar system is filled with plasma such as the solar wind, solar and galactic cosmic rays (high energy charged particles), and particles trapped in the planetary magnetospheres. The first in situ observations of plasma and energetic particle populations in the magnetospheres of Jupiter, Saturn, Uranus, Neptune, and Titan were made by the Voyager 1 and 2 spacecraft from 1979 to 1989. Interplanetary spacecraft have identified magnetospheres around Mercury, Venus, Jupiter, Saturn, Uranus, and Neptune.

Comets also have "magnetospheres." The cometosheath, a region extending about 1.1×10^6 km (for Comet Halley), consists of decelerated plasma of density and temperature $T_e \sim 1.5$ eV. The peak magnetic field strength found in Comet Halley was 700-800 mG. Confirmation that pinched Birkeland currents also occur in cometary magntospheres was obtained by the detection of X rays from Comet Hyakutake in 1996.

Excluding the Sun, the largest organized structures found in the solar system are the plasma tori around Jupiter and Saturn. The Jupiter-Io plasma torus is primarily filled with sulphur ions at a density of 3×10^3 cm^{-3}. An immense weakly ionized hydrogen plasma torus has been found to encircle Saturn, with an outer diameter 25 times the radius of the planet and an inner diameter of about fifteen Saturn radii.

2.2.4. *Transition Regions in the Solar System*

Examples of transition regions include the boundary layers found in planetary and comet magnetospheres. Transition regions between plasmas of different densities, temperatures, magnetization, and chemical composition offer a rich variety of plasma phenomena in the solar system [Eastman 1990].

2.2.5. *Solar, Stellar, and Interstellar Plasmas*

The nuclear core of the Sun is a plasma at about a temperature of 1.5 keV. Beyond this, our knowledge about the Sun's interior is highly

uncertain. Processes which govern the abundance of elements, nuclear reactions, and the generation mechanism and strength of the interior magnetic fields, are incompletely known.

We do have information about the Sun's surface atmospheres that are delineated as follows: the photosphere, the chromosphere, and the inner corona. These plasma layers are superposed on the Sun like onion skins. The photosphere ($T \sim 0.5$ eV) is only a very weakly ionized atmosphere, the degree of ionization being $10^{-4} - 10^{-5}$ in the quiet regions and perhaps $10^{-6} - 10^{-7}$ in the vicinity of sunspots. The chromosphere ($T \sim 4$ eV) extends 5,000 km above the photosphere and is a transition region to the inner corona. The highly ionized inner corona extends some 10^5 km above the photosphere. From a plasma physics point of view, the corona is perhaps the most interesting region of the Sun. The corona is the sight of explosively unstable magnetic-field configurations, X ray emission, and plasma temperatures in the range 70-263 eV.[4] The source of this heating is uncertain.[5]

Solar flares resulting from coronal instabilities raise temperatures to 10-30 keV and produce relativistic streams of electrons and protons. Particles accelerated outward produce radio interference at the earth. Protons accelerated inward collide with ions in the Sun's atmosphere to produce nuclear reactions, whose gamma rays and neutrons have been detected from spacecraft. Solar flares consist of plasma at a temperature of about 1 keV to 10 keV. Although flares represent the most intense energy dissipation of any form of solar activity, releasing energy in the form of gamma rays, X rays, and microwaves, the active sun has many other plasma manifestations.

These include sunspots, photospheric faculae, chromospheric and transition region plages, large coronal loops, and even larger scale coro-

[4] One of the Sun's outstanding problems is the temperature of the corona. The temperature rises steadily in the chromosphere, then jumps abruptly in the corona to a level 300 times hotter than the surface. That the Sun is a plasma and not just a hot gaseous object is illustrated by the fact that the temperature increases away from its surface, rather than cooling as dictated by the thermodynamic principle for matter in the nonplasma state.

[5] For decades the preferred explanation has been that energy flows from the Sun's surface to the corona in the form of sound waves generated by convective upswelling motions. However, space-based ultraviolet observations proved that sound waves do not carry energy as high as the corona. One mechanism that may produce coronal heating is electron beams produced in double layers in coronal loops. These are expected to accelerate electrons to energies comparable to those in the corona. Generally, the term acceleration refers to the preferential gain of energy by a population of electrons and ions, while heating is defined as the bulk energization of the ambient plasma. Paraphrasing Kirchoff that "heating is a special kind of acceleration," one may argue, since heating and acceleration are always present in flares and in laboratory relativistic electron beams, that electron beam instabilities may be the source of coronal heating.

nal streamers and occasional coronal mass ejections. In addition, prominences (referred to as filaments when seen in H_α absorption on the disk) frequently form between opposite magnetic polarities in active regions of the sun. These phenomena are dynamic, on time scales ranging from seconds to the complete solar magnetic cycle of 22 years.

The outer corona and solar wind form the heliosphere. At one astronomical unit the solar wind has a plasma density $5 \leq n \leq 60$ cm-3 and a velocity of $200 \leq v_{sw} \leq 800$km s^{-1}. Its temperature can be as high as 50 eV, while B may reach 200 mG. The outer heliosphere has a plasma density $10^{-3} \leq n \leq 10^{-1}$ cm^3, a temperature $10^{-1} \leq T < 10$ eV, and a magnetic field strength ~ 1 mG. The local interstellar medium is characterized by $10^{-2} \leq n \leq 1$, a temperature of order 1 eV, and magnetic field strength $1 \leq B \leq 20\mu$G.

The rotating sun, coupled with its continual radial ejection of plasma, twists its magnetic field (that is referred to as the interplanetary magnetic field or IMF) into a classical Archimedean spiral. Measurements have confirmed that the interplanetary magnetic field is directed toward the sun in certain regions of the solar system and away from the sun in other regions. These regions are separated by a very sharp boundary layer that is interpreted as a current layer. In this situation, the planets find themselves sometimes in a region where the field has a strong northward component and sometimes where it has a strong southward component.

Stellar plasmas have not only the dimension of the star, 0.3×10^6 km to 10^8 km, but also the stellar magnetospheres, a remnant of the interstellar plasma that the star and its satellites condensed out of. The surface temperatures vary from about 0.3 to 3 eV. Estimates of the magnetic fields range from a few gauss to tens of kilogauss or more for magnetic variable stars.

Stellar winds occur in stars of many types, with wind properties probably connected with stellar magnetism.

2.2.6. *Galactic and Extragalactic Plasmas*

Dark clouds within our Galaxy have dimensions of 10^8 km and microgauss strength magnetic fields.

The Galactic plasma has an extent equal to the dimensions of our Galaxy itself; $\sim$35 kpc or 10^{21} m. The most salient feature of the Galactic plasma are 10^{-3} G poloidal-toroidal plasma filaments extending nearly 250 light years (60 pc, 1.8×10^{18} m) at the Galactic center. The vast regions of nearly neutral hydrogen (HI regions) found in the Galaxy and other galaxies are weakly ionized plasmas. These regions extend across the entire width of the galaxy and are sometimes found

between interacting galaxies. They are detected by the 21 cm radiation they emit.

Galaxies may have bulk plasma densities of 10^{-1} cm^{-3}; groups of galaxies, 3×10^{-2} cm^{-3}; and rich clusters of galaxies, 3×10^{-3} cm^{-3}.

By far the single largest plasmas detected in the Universe are those of double radio galaxies. In size, these sources extend hundreds of kiloparsecs ($10^{21} - 10^{22}$ m) to a few megaparsecs ($10^{22} - 10^{23}$ m). Double radio galaxies are thought to have densities of 10^{-3} cm^{-3} and magnetic fields of the order of 10^{-4} G.

2.3. Regions of Applicability of Plasma Physics

The degree of ionization in interplanetary space and in other cosmic plasmas may vary over a wide range, from fully ionized to degrees of ionization of only a fraction of a percent.[6] Even weakly ionized plasma reacts strongly to electromagnetic fields since the ratio of the electromagnetic force to the gravitational force is 39 orders of magnitude. For example, although the solar photospheric plasma has a degree of ionization as low as 10^{-4}, the major part of the condensible components is still largely ionized. The "neutral" hydrogen (HI) regions around galaxies are also plasmas, although the degree of ionization is only 10^{-4}. Most of our knowledge about electromagnetic waves in plasmas derives from laboratory plasma experiments where the gases used have a low degree of ionization, 10^{-2}-10^{-6}.

Because electromagnetic fields play such an important role in the electrodynamics of plasmas, and because the dynamics of plasmas are often the sources of electromagnetic fields, it is desirable to determine where within the universe a plasma approach is necessary. We first consider the magnetic field. The criterion for neglecting magnetic effects in the treatment of a problem in gas dynamics is that the Lundquist parameter is much less than unity,

$$L_u = \frac{u^{1/2}\sigma B l_c}{\sqrt{\rho_m}} << 1 \tag{6}$$

where l_c is a characteristic length of the plasma and ρ_m is the mass density. As the conductivity of known plasmas generally varies only over about four orders of magnitude, from 10^2 to 10^6 siemens/m, the value of is largely dependent on the strength of B in the plasma.

The variation of B in plasmas can be 18 orders of magnitude, from microgauss strengths in intergalactic space to perhaps teragauss levels in the magnetospheres of neutron sources. On earth, magnetic field

[6] The degree of ionization is defined as $n_p/(n_0 + n_p)$ where n_p is the plasma density and n_0 is the density of neutral particles.

strengths can be found from about 0.5 gauss (0.5×10^{-4} T) to 10^7 gauss (10^3 T) in pulsed-power experiments; the outer planets have magnetic fields reaching many gauss, while the magnetic fields of stars are 30-40 kG (3-4 T). Large scale magnetic fields have also been discovered in distant cosmic objects. The center of the Galaxy has milligauss magnetic field strengths stretching 60 pc in length. Similar strengths are inferred from polarization measurements of radiation recorded for double radio galaxies. No rotating object in the universe, that is devoid of a magnetic field, is known.

In cosmic problems involving planetary, interplanetary, interstellar, galactic, and extragalactic phenomena, L_u is usually of the order $10^{15} - 10^{20}$. In planetary ionospheres falls below unity in the E layer. Neglecting lightning, planetary atmospheres and hydrospheres are the only domains in the universe where a nonhydromagnetic treatment of fluid dynamic problems is justified.

2.3.1. *Field-Aligned Currents in Astrophysical Plasmas*

As far as we know, most cosmic low density plasmas also depict a filamentary structure. For example, filamentary structures are found in the following cosmic plasmas, all of which are observed or are likely to be associated with electric currents:

1. In the aurora, filaments parallel to the magnetic field are often observed. These can sometimes have dimensions down to about 100 m.

2. Inverted V events and the in-situ measurements of strong electric fields in the magnetosphere ($10^5 - 10^6$ A, 10^8 m) demonstrate the existence of filamentary structures.

3. In the ionosphere of Venus, "flux ropes", whose filamentary diameters are typically 20 km, are observed.

4. In the sun, prominences (10^{11} A), spicules, coronal streamers, polar plumes, etc., show filamentary structure whose dimensions are of the order $10^7 - 10^8$ m.

5. Cometary tails often have a pronounced filamentary structure.

6. In the interstellar medium and in interstellar clouds there is an abundance of filamentary structures [e.g., the Veil nebula, the Lagoon nebula, the Orion nebula, and the Crab nebula].

7. The center of the Galaxy, where twisting plasma filaments, apparently held together by a magnetic field possessing both azimuthal and poloidal components, extend for nearly 60 pc (10^{18} m).

8. Within the radio bright lobes of double radio galaxies, where filament lengths may exceed 20 kpc (6×10^{20} m).

9. In extended radio sources and synchrotron emitting jets [Gouveia Dal Pino and Olpher 1989]

Regardless of scale, the motion of charged particles produces a self-magnetic field that can act on other collections of particles or plasmas, internally or externally. Plasmas in relative motion are coupled via currents that they drive through each other. Currents are therefore expected in a universe of inhomogeneous astrophysical plasmas of all sizes.

3. Dynamical Characteristics of Plasmas

It is the global dynamics and systematic interactions of astrophysical plasmas that allow energy to be conveyed over great distances. The evolution of cosmic plasma that includes its structuring into cells results in a relative motion, however slow, of plasma clouds whose dimensions may be measured in hundreds or megaparsecs or gigaparsecs. All plasma clouds may be considered a system: they are coupled by electrical currents (charged particles beams) they induce in each other. These beams are the source of energy transfer from large, slow moving plasma to smaller plasma regions that may release the energy abruptly or cause local plasmas to pinch to the condense state.

3.1. Power Generation and Transmission

On earth, power is generated by nuclear and nonnuclear fuels, hydro and solar energy, and to a much lesser extent, by geothermal sources and magnetohydrodynamic generators. Always, the location of the supply is not the location of major power usage or dissipation. Transmission lines are used to convey the power generated to the load region. As an example, abundant hydroelectric resources in the Pacific Northwest of the United States produce power (~1,500 MW) that is then transmitted to Los Angeles, 1,330 km away, via 800 kV high-efficiency dc transmission lines. In optical and infrared emission, only the load region, Los Angeles, is visible from the light and heat it dissipates in power usage. The transmission line is invisible.

This situation is also true in space. With the coming of the space age and the subsequent discovery of magnetospheric-ionospheric electrical circuits, Kirchoff's circuit laws were suddenly catapulted to dimensions eight orders of magnitude larger than that previously investigated in

the laboratory and nearly four orders of magnitude greater than that associated with the longest power distribution systems on earth.

On earth, transmission lines consist of metallic conductors or waveguides in which energy is made to flow via the motion of free electrons (currents) in the metal or in displacement currents in a time varying electric field. Often strong currents within the line allow the transmission of power many orders of magnitude stronger than that possible with weak currents. This is because a current associated with the flow of electrons produces a self-magnetic field that helps to confine or pinch the particle flow. Magnetic-insulation is commonly used in pulsed-power technology to transmit large amounts of power from the generator to the load without suffering a breakdown due to leakage currents caused by high electric potentials.

There is a tendency for charged particles to follow magnetic lines of force and this forms the basis of transmission lines in space. In the magnetosphere-ionosphere, a transmission line 7-8 earth radii in length (R_e = 6,350 km) can convey tens of terawatts of power, that derives from the solar wind-magnetosphere coupling[7], to the lower atmosphere. The transmission line is the earth's dipole magnetic field lines along which electrons and ions are constrained to flow. The driving potential is solar-wind induced plasma moving across the magnetic field lines at large radii. The result is an electrical circuit in which electric currents cause the formation of auroras at high latitude in the upper atmosphere on earth. This aurora mechanism is observed on Jupiter, Io, Saturn, Uranus, and is thought to have been detected on Neptune and perhaps, Venus.

Only the aurora discharge is visible at optical wavelengths to an observer. The source and transmission line are invisible. Before the coming of space probes, in situ measurement was impossible and exotic explanations were often given of auroras. This is probably true of other non in situ cosmic plasmas today. The existence of a megaampere flux tube of current, connecting the Jovian satellite Io to its mother planet, was verified with the passage of the Voyager spacecraft.

3.2. Electrical Discharges in Cosmic Plasma

An electrical discharge is a sudden release of electric or magnetic stored energy. This generally occurs when the electromagnetic stress exceeds some threshold for breakdown that is usually determined by small scale

[7] It is not known how the energy carried by the solar wind is transformed into the energy of the aurora. It has been demonstrated that the southward-directed interplanetary magnetic field is an essential ingredient in causing auroral substorms so that energy transformation appears to occur through interactions between the interplanetary and geomagnetic fields [Akasofu 1981].

properties of the energy transmission medium. As such, discharges are local phenomena and are usually accompanied by violent processes such as rapid heating, ionization, the creation of pinched and filamentary conduction channels, particle acceleration [Melrose 1997], and the generation of prodigious amounts of electromagnetic radiation.

As an example, multi-terawatt pulsed-power generators on earth rely on strong electrical discharges to produce intense particle beams, X rays, and microwaves. Megajoules of energy are electrically stored in capacitor banks, whose volume may encompass 250 m^3. This energy is then transferred to a discharge region, located many meters from the source, via a transmission line. The discharge region, or load, encompasses at most a few cubic centimeters of space, and is the site of high-variability, intense, electromagnetic radiation.

On earth, lightning is another example of the discharge mechanism at work where electrostatic energy is stored in clouds whose volume may be of the order of 3,000 km^3. This energy is released in a few cubic meters of the discharge channel.

The aurora is a discharge caused by the bombardment of atoms in the upper atmosphere by 1-20 keV electrons and 200 keV ions spiraling down the earth's magnetic field lines at high latitudes. Here, the electric field accelerating the charged particles derives from plasma moving across the earth's dipole magnetic field lines many earth radii into the magnetosphere. The potential energy generated by the plasma motion is fed to the upper atmosphere by multi-megaampere Birkeland currents that comprise a transmission line, 50,000 kilometers in length, as they flow into and out of the discharge regions at the polar horns. The generator region may encompass $10^{12} - 10^{13}$ km^3 while the total discharge volume can be $10^9 - 10^{10}$ km^3.

3.2.1. *Flickering of Electromagnetic Radiation*

The flickering of a light in Los Angeles does not mean that the *supply source*, a waterfall or hydroelectric dam in the Pacific Northwest, has abruptly changed dimensions or any any other physical property. The flickering comes from electrical changes at the observed load or *radiative source*, such as the formation of instabilities or virtual anodes or cathodes in charged particle beams that are orders of magnitude smaller than the supply. Bizarre and interesting non-physical interpretations are obtained if the flickering light is interpreted by a distant observer to be both the source and supply. This also holds true for astrophysical plasmas. The flickering and pulsating of the observed electromagnetic radiation from a distant astrophysical source, when interpreted to be local, unattached, and isolated in 'vacuum' space, leads to bizarre 'black hole' type explanations. As discussed earlier, space is not vacu-

um but rather filled with plasma whose properties, volume-wise, differ little from those in the laboratory or magnetospheres. And plasmas exhibit large *system* global properties, such as the transfer of energy over great distances to smaller regions where it may be systematically or catastrophically released.

3.3. Particle Acceleration in Cosmic Plasma

3.3.1. *Acceleration of Electric Charges*

The acceleration of a charged particle q in an electromagnetic field is mathematically described by the Lorentz equation Eq. 5,

$$\mathbf{F} = m\mathbf{a} = q\,(\mathbf{E} + \mathbf{v} \times \mathbf{B}) \tag{7}$$

The electric field vector $\mathbf{E}$ can arise from a number of processes that include the motion of plasma with velocity $\mathbf{v}$ across magnetic fields lines $\mathbf{B}$, charge separation, and time varying magnetic fields via Eq. 1.

Acceleration of charged particles in laboratory plasmas is achieved by applying a potential gradient between metallic conductors (cathodes and anodes); by producing time varying magnetic fields such as in betatrons; by radio frequency (RF) fields applied to accelerating cavities as in linear accelerators (LINACS); and by beat frequency oscillators or wake-field accelerators that use either the electric field of lasers or charged particle beams to accelerate particles.

The magnetospheric plasma is essentially collisionless. In such a plasma, electric fields aligned along the magnetic field direction freely accelerate particles. Electrons and ions are accelerated in opposite directions, giving rise to a current along the magnetic field lines.

3.3.2. *Collective Ion Acceleration*

The possibility of producing electric fields by the space-charge effect to accelerate positive ions to high energies was first discussed by Alfvén and Wernholm in 1952. They were unsuccessful in their attempt to experimentally accelerate ions in the collective field of clouds of electrons, probably because of the low intensity of electron beam devices available then. However, proof of principle came in 1961 when Plyutto reported the first successful experiment in which ions were collectively accelerated. By 1975, the collective acceleration of ions had become a wide-spread area of research. Luce reported collectively accelerating both light and heavy ions to multi-MeV energies, producing an intense burst of D-D neutrons and nuclear reactions leading to the identification of several radioisotopes. Luce used a plasma-focus device and attributed the collective beam to intense current vortex filaments in the pinched plasma. Subsequently in 1979, Destler, Hoeberling, Kim,

and Bostick collectively accelerated carbon ions to energies in excess of 170 MeV using a 6 MeV electron beam.

Individual ion energies up to several GeV using pulsed-power generators have been suggested in particle-in-cell simulations of collective ion acceleration processes.

Collective acceleration as a mechanism for creating high energy ions in astrophysical plasmas were investigated by Bostick [1986].

3.4. Plasma Pinches and Instabilities

3.4.1. *The Bennett Pinch*

In cosmic plasma the perhaps most important constriction mechanism is the electromagnetic attraction between parallel currents. A manifestation of this mechanism is the pinch effect as first studied by Bennett (1934). Phenomena of this general type also exist on a cosmic scale and lead to a bunching of currents and magnetic fields to filaments. This bunching is usually accompanied by the accumulation of matter, and it may explain the observational fact that cosmic matter exhibits an abundance of filamentary structures.

Consider a fully ionized cylindrical plasma column of radius r, in an axial electric field E_z, that produces an axial current density j_z. Associated with j_z is an azimuthal magnetic field B_ϕ. The current flowing across its own magnetic field exerts a $\mathbf{j} \times \mathbf{B}$, radially inward, pinch force. In the steady-state, the balance of forces is

$$\nabla p = \nabla (p_e + p_i) = \mathbf{j} \times \mathbf{B} \tag{8}$$

By employing Eq. 2, $\nabla \times \mathbf{B} = \mu_0 \mathbf{j}$, and the perfect gas law $p = NkT$, we arrive at the Bennett relation

$$2Nk (T_e + T_i) = \frac{\mu_0}{4\pi} I^2 \tag{9}$$

where N is the number of electrons per unit length along the beam, T_e and T_i are the electron and ion temperatures, I is the total beam current, and k is Boltzmann's constant.

3.4.2. *The Force-Free Configuration*

Sheared magnetic fields are a characteristic of most plasmas. Here, the sheared field is considered a nonpotential field that is caused by shear flows of plasma. A nonpotential field tends to settle into a particular configuration called a "force-free" field, namely

$$(\nabla \times \mathbf{B}) \times \mathbf{B} = 0 \tag{10}$$

or

$$\mathbf{j} \times \mathbf{B} = 0 \tag{11}$$

since $\mathbf{j} = \nabla \times \mathbf{B}\mu_0^{-1}$, showing that the electric current tends to flow along $\mathbf{B}$. Substituting 11 into 8 gives $\mathbf{F} = \nabla p = 0$, hence the name "force-free". Force-free fields tend to have a twisted or "sheared" appearance. Examples of force-free fields are chromospheric fibrils and penumbral structures near active sunspots.

The condition 10 can be satisfied in three ways: $\mathbf{B} = \mathbf{0}$ (trivial), (i.e., $\mathbf{j} = \mathbf{0}$), or

$$\nabla \times \mathbf{B} = \alpha \mathbf{B} \tag{12}$$

where the scalar $\alpha = \alpha(r)$ in general. The essence of a force-free field is simply that electric currents flow parallel to magnetic field lines. Such currents are often called "field-aligned" currents.

The force-free fields with constant α represent the lowest state of magnetic energy that a closed system may attain. This has two important consequences. It proves the stability of force-free fields with constant α, and shows that in a system in which the magnetic forces are dominant and in which there is a mechanism to dissipate the fluid motion, force-free fields with constant α are the natural end configuration. In astrophysical plasmas, the dissipation mechanism may be the acceleration of charged particles to cosmic ray energies.

3.5. Analysis of Beams and Filamentary Plasma

3.5.1. *General Plasma Fluid Equations*

Fundamental equations for the plasma velocity, magnetic field, plasma density, electric current, plasma pressure, and plasma temperature can be derived from macroscopic averages of currents, fields, charge densities, and mass densities. In this "fluid" treatment, the Maxwell's equations 1- 4 are coupled to the moments of the Boltzmann equation for a highly ionized plasma.

The evolution of the distribution function $f(\mathbf{r}, \mathbf{p}, t)$ for particles with charge q and mass m is described by the Boltzmann equation

$$\left[\frac{\partial}{\partial t} + \mathbf{v} \cdot \frac{\partial}{\partial \mathbf{r}} + q\left(\mathbf{E} + \mathbf{v} \times \mathbf{B}\right) \cdot \frac{\partial}{\partial \mathbf{p}}\right] f\left(r, p, t\right) = \left(\frac{\partial f}{\partial t}\right)_{collisions} \tag{13}$$

which is an expression of Liouville's theorem for the incompressible motion of particles in the six-dimensional phase space $(\mathbf{r}, t)$. In the fluid description the particle density n, mean velocity $\bar{v}$, momentum $n\bar{v}$, pressure P, and friction R are defined by

$$n(r,t) \equiv \int d^3p f(r,p,t) \tag{14}$$

$$n(r,t)\,\bar{v}(r,t) \equiv \int d^3p v f(r,p,t) \tag{15}$$

$$n(r,t)\,\bar{p}(r,t) \equiv \int d^3p p f(r,p,t) \tag{16}$$

$$P(r,t) \equiv \int d^3p\,[\bar{p} - p(r,t)]\,[\bar{v} - v(r,t)]\,f(r,p,t) \tag{17}$$

$$R(r,t) \equiv \int d^3p\,[\bar{p} - p(r,t)] \left(\frac{\partial f}{\partial t}\right)_{collisions} \tag{18}$$

where the momentum p and velocity v are related by

$$p = m\gamma v \tag{19}$$

The fields $E(r,t)$ and $B(r,t)$ in Eq. 13 are self-consistently solved from Eqs. 1- 4 with

$$\rho(r,t) \equiv e \int d^3p f(r,p,t) \tag{20}$$

$$j(r,t) \equiv e \int d^3p v f(r,p,t) \tag{21}$$

Taking the moments $\int d^3p$ and $\int d^3p\mathbf{p}$ of the Boltzmann equation yields the two-fluid equations [Alfvén and Fälthammar 1963] for ions and electrons $\alpha = i, e$,

$$\frac{\partial n_\alpha}{\partial t} + \nabla \cdot (n_\alpha \bar{v}_\alpha) = 0 \tag{22}$$

$$n_\alpha \frac{dp_\alpha}{dt} = q_\alpha n_\alpha (E + v_\alpha \times B) - \nabla \cdot P_\alpha + R_\alpha - n_\alpha m_\alpha \nabla \phi_G \tag{23}$$

These are called the continuity and momentum equations, respectively. The continuity equation, as written, is valid if ionization and recombination are not important. Conservation of linear momentum dictates that

$$R_i + R_e = 0 \tag{24}$$

The two fluid equations are the moments, or averages, of the kinetic plasma description and no longer contain the discrete particle phenomena such as double layers from charge separation and synchrotron

radiation. Nevertheless, this approach is useful in studying bulk plasma flow and behavior. A single fluid hydromagnetic force equation may be obtained by substituting into Eq. 23 and adding to get,

$$\rho_m \frac{\partial \mathbf{v}_m}{\partial t} = \rho \mathbf{E} + \mathbf{j} \times \mathbf{B} - \nabla p - \rho_m \nabla \phi_G \tag{25}$$

which relates the forces to mass and acceleration for the following averaged quantities:

$$\begin{array}{cc} \rho_m = n_e m_e + n_i m_i & \text{mass density} \\ \mathbf{j}_m = n_e m_e \bar{\mathbf{v}}_e + n_i m_i \bar{\mathbf{v}}_i & \text{mass current} \\ \mathbf{v}_m = \mathbf{j}_m / \rho_m & \text{averaged velocity} \\ \rho = n_e q_e + n_i q_i & \text{charge density} \\ \mathbf{j} = n_e q_e \bar{\mathbf{v}}_e + n_i q_i \bar{\mathbf{v}}_i & \text{current density} \end{array} \tag{26}$$

The first term in Eq. 26 is caused by the electric field, the second term derives from the motion of the current flow across the magnetic field, the third term is due to the pressure gradient [Eq. 26 is valid for an isotropic distribution $\nabla \cdot P \rightarrow \nabla p$, where $p \equiv nkT$], and the fourth term is due to the gravitational potential φ_G. The near absence of excess charge $\rho = e\,(n_i - n_e) \approx 0$, for $q_{i,e} = \pm e$, is a characteristic of the plasma state; however, this does not mean that electrostatic fields [e.g., those deriving from Eq. 3] are unimportant. According to Chen [1985]:

> "In a plasma, it is usually possible to assume $n_i = n_e$ and $\nabla \cdot \mathbf{E} \neq 0$ at the same time. We shall call this the *plasma approximation.* It is a fundamental trait of plasmas, one which is difficult for the novice to understand. *Do not use Poisson's equation to obtain E unless it is unavoidable!*"

Completing the single fluid description is the equation for mass conservation,

$$\frac{\partial \rho_m}{\partial t} + \nabla \cdot (\rho_m \mathbf{v}_m) = 0 \tag{27}$$

In addition to Eqs. 25 and 27, we find it useful to add the equation for magnetic induction,

$$\frac{\partial B}{\partial t} = \nabla \times (\mathbf{v}_m \times \mathbf{B}) + \frac{1}{\mu\sigma} \nabla^2 B \tag{28}$$

obtained by taking the curl of Ohm's law

$$\mathbf{j} = \sigma\,(\mathbf{E} + \mathbf{v} \times \mathbf{B})$$

where σ is the electrical conductivity.

3.5.2. *Magnetic Reynolds and Lundquist Numbers*
The significance of Eq. 28 in which $(\mu\sigma)^{-1}$ is the magnetic diffusivity, is that changes in the magnetic field strength are caused by the transport of the magnetic field with the plasma (as represented by the first term on the right-hand-side), together with diffusion of the magnetic field through the plasma (second term on the right-hand-side). In order of magnitude, the ratio of the first to the second term is the *magnetic Reynolds number*

$$R_m = \mu\sigma V_c l_c \tag{29}$$

in terms of a characteristic plasma speed V_c and a characteristic scale length l_c. A related quantity is the Lundquist parameter

$$L_u = \mu\sigma V_A l_c \tag{30}$$

where

$$V_A = \frac{B}{\sqrt{\mu\rho_m}} \tag{31}$$

is the Alfvén speed. It may be written as the ratio

$$L_u = \frac{\tau_d}{\tau_A} \tag{32}$$

of the *magnetic diffusion time*

$$\tau_d = \mu\sigma l_c^2 \tag{33}$$

to the *Alfvén travel time*

$$\tau_A = l_c/V_A \tag{34}$$

3.6. The Generalized Bennett Relation

A generalized Bennett relation follows directly from Eq. 25 and Eqs. 1-4. Consider a current-carrying, magnetic-field-aligned cylindrical plasma of radius a which consists of electrons, ions, and neutral gas having the densities n_e, n_i, and n_n, and the temperatures T_e, T_i, and T_n, respectively. A current of density j_z flows in the plasma along the axis of the cylinder which coincides with the z-axis. As a result of the axial current a toroidal magnetic field B_ϕ is induced. An axial electric field is also present. Thus, there exists the electric and magnetic fields

$$\mathbf{E} = (E_r, E_\phi, E_z)$$
$$\mathbf{B} = (0, B_\phi, B_z)$$

The derivation of the generalized Bennett relation for this plasma is straightforward, but lengthy [Witalis 1981], and the final result is

$$\begin{aligned} \tfrac{1}{4}\tfrac{\partial^2 J_0}{\partial t^2} &= W_\perp + \Delta W_{E_z} + \Delta W_{B_z} + \Delta W_k \\ -\tfrac{\mu_0}{8\pi} I^2(a) - \tfrac{1}{2} G \bar{m}^2 N^2(a) &+ \tfrac{1}{2}\pi a^2 \varepsilon_0 \left(E_r^2(a) - E_\phi^2(a)\right) \end{aligned} \tag{35}$$

where

$$J_0 = \int_0^{2\pi} \int r^2 \rho_m r dr d\phi = \int_0^a r^2 \rho_m 2\pi r dr \tag{36}$$

is the total moment of inertia with respect to the z axis. (As the mass m of a particle or beam is its resistance to linear acceleration, J_0 is the beam resistance to angular displacement or rotation). The quantities ΔW are defined by

$$\Delta W_{E_z} \equiv W_{E_z} - \frac{1}{2}\varepsilon_0 E_z^2(a)\,\pi a^2 \tag{37}$$

$$\Delta W_{B_z} \equiv W_{B_z} - \frac{1}{2\mu_0} B_z^2(a)\,\pi a^2 \tag{38}$$

$$\Delta W_k \equiv W_k - p(a)\,\pi a^2 \tag{39}$$

where $E_z(a)$, $B_z(a)$, and $p(a)$ denote values at the boundary $r = a$. The individual energies W are defined as follows. The kinetic energy per unit length due to beam motion transverse to the beam axis:

$$W_{\perp\ kin} \equiv \frac{1}{2}\int_0^a \rho_m(r)\left[v_\phi^2 + v_r^2\right] 2\pi r dr \tag{40}$$

The self-consistent B_z energy per unit length:

$$W_{B_z} \equiv \frac{1}{2\mu_0}\int_0^a B_z^2(r)\, 2\pi r dr \tag{41}$$

The self-consistent E_z energy per unit length:

$$W_{E_z} \equiv \frac{\varepsilon_0}{2}\int_0^a E_z^2(r)\, 2\pi r dr \tag{42}$$

The thermokinetic energy per unit length:

$$W_k \equiv \int_0^a p(r)\, 2\pi r dr \tag{43}$$

The axial current inside the radius a:

$$I(a) \equiv \int_0^a j_z(r)\, 2\pi r dr \tag{44}$$

The total number of particles per unit length:

$$N(a) \equiv \int_0^a n(r)\, 2\pi r dr \tag{45}$$

where $n = n_i + n_e + n_n$ is the total density of ions, electrons, and neutral particles. The mean particle mass is $\bar{m} = n_i m_i + n_e m_e + n_n m_n$. The self-consistent electric field can be determined from the following equation,

$$r^{-1}\frac{d(rE_r)}{dr} = -\frac{e}{\varepsilon_0}(n_e - n_i)$$

and is given by

$$E_r(r) = \frac{-en_e(1-f_e)}{2\varepsilon_0} r,\ 0 \le r \le a$$

$$E_r(r) = \frac{-en_e(1-f_e)}{2\varepsilon_0}\frac{a^2}{r},\ r \ge a$$

Neglecting the displacement current, the self-consistent magnetic field can be determined from Ampère's law Eq. 2,

$$r^{-1}\frac{d(rB_\phi)}{dr} = \mu_0 j$$

and is given by

$$B_\phi(r) = \frac{\mu_0 I}{2\pi}\frac{r}{a^2},\ 0 \le r \le a$$

$$= \frac{\mu_0 I}{2\pi r},\ r \ge a$$

The positive terms in Eq. 35 are expansional forces while the negative terms represent beam compressional forces. In addition, it is assumed that the axially directed kinetic energy is

$$W_{||kin} = \frac{1}{2}\gamma m N \beta^2 c^2 \tag{46}$$

Since Eq. 35 contains no axially directed energy, it must be argued that there are conversions or dissipation processes transferring a kinetic beam of energy of magnitude $W_{||kin}$ into one or several kinds of energy expressed by the positive W elements in Eq. 35:

$$W_{||kin} = W_{\perp\ kin} + W_{E_z} + W_{B_z} + W_k \tag{47}$$

3.6.1. *The Bennett Relation*
Balancing the thermokinetic and azimuthal compressional (pinch) energies in Eq. 35,

$$W_k - \frac{\mu_0}{8\pi} I^2 = 0 \tag{48}$$

yields the Bennett relation,

$$\frac{\mu_0}{4\pi} I^2 = 2NkT \tag{49}$$

If there is a uniform temperature $T = T_e + T_i$ and if the current density is uniform across the current channel cross-section, Eqs. 44, 45, and 49 yield a parabolic density distribution

$$n(r) = \frac{\mu_0 I^2}{4\pi^2 a^2 kT}\left(1 - \frac{r^2}{a^2}\right)$$

3.6.2. *Alfvén Limiting Current*
Equating the parallel beam kinetic energy to the pinch energy

$$W_{\perp\ kin} - \frac{\mu_0}{8\pi} I^2 = 0 \tag{50}$$

yields the Alfvén limiting current

$$I_A = 4\pi\varepsilon_0 m_e c^3 \beta\gamma / e = 17\beta\gamma \text{ kiloamperes} \tag{51}$$

for an electron beam. This quantity was derived by Alfvén in 1939 in order to determine at what current level in a cosmic ray beam the self-induced pinch field would turn the forward propagating electrons around. It should be noted that this limit is independent of any physical dimensions.

Lawson's (1959) interpretation of Eq. 51 is that the electron trajectories are beam-like when $I < I_A$ and they are plasma-like when

$I > I_A$. In laboratory relativistic electron beam (REB) research, Budker's parameter

$$\nu_{Bud} = \pi a^2 n_b e^2/mc^2 = Ne^2/mc^2 \tag{52}$$

where n_b is the electron density of the beam, finds wide application in beam and plasma accelerators. Yonas (1974) has interpreted the particle trajectories as beam-like for $\nu_{Bud} < \gamma$ and plasma-like for $\nu_{Bud} > \gamma$. The relationship between I_A and ν_{Bud} is

$$\nu_{Bud}/\gamma = I/I_A \tag{53}$$

The Alfvén limiting current Eq. 51 is a fundamental limit for a uniform beam, charge-neutralized ($f_e = 1$), with no magnetic neutralization ($f_m = 0$), no rotational motion ($v_\phi = 0$), and no externally applied magnetic field ($B_z = 0$). By modifying these restrictions, it is possible, under certain circumstances, to propagate currents in excess of I_A.

3.6.3. *Charge Neutralized Beam Propagation*

Balancing the parallel kinetic, pinch, and radial electric field energies in Eq. 35 gives

$$W_{\perp\ kin} - \frac{\mu_0}{8\pi} I^2 + \frac{1}{2}\pi a^2 \varepsilon_0 E_r^2\,(a) = 0 \tag{54}$$

which yields[8]

$$I_{\max} = I_A \beta^2 \left[\beta^2 - (1 - f_e)^2\right]^{-1},\ 0 \le f_e \le 1 \tag{55}$$

Depending on the amount of neutralization, the denominator in Eq. 55 can become small, and I_{max} can exceed I_A. However, the unneutralized electron beam cannot even be injected into a drift space unless the space charge limiting current condition is satisfied. For a shearless electron beam this is [Bogdankevich and Rukhadze 1971]

$$I_{sc} = \frac{17\left(\gamma^{2/3} - 1\right)^{3/2}}{1 + 2\ln\,(b/a)}\ \ kiloamperes \tag{56}$$

where b is the radius of a conducting cylinder surrounding the drift space. Thus, in free space $I_{sc} \to 0$ and an unneutralized electron beam

[8] This equation differs from the Alfvén-Lawson limiting current, $I_{\max} = I_A\beta^2/\left[\beta^2 - 1 + f_e\right]$, because of the differing ways in describing charge neutralization [Witalis 1981].

will not propagate but, instead, builds up a space charge cloud of electrons (a virtual cathode) which repels any further flow of electrons as a beam. Moreover, the space charge limiting current is derived under the assumption of an infinitely large guide field B_z; no amount of magnetic field will improve beam propagation.

3.6.4. *Current Neutralized Beam Propagation*
For beam propagation in plasma, the electrostatic self-field E_z built up by the beam, efficiently drives a return current through the plasma, thus moderating the compressional term $\mu_0 I^2/8\pi$ in Eq. 35, so that

$$W_{\perp\ kin} - \frac{\mu_0}{8\pi} I^2 (1 - f_m) + \frac{1}{2}\pi a^2 \varepsilon_0 E_r^2 (a) = 0 \tag{57}$$

where the magnetic neutralization factor is

$$f_m \equiv |I_{return}/I| \tag{58}$$

From Eq. 57 the maximum current is

$$I_{\max} = I_A \beta^2 \left[\beta^2 (1 - f_m) - (1 - f_e)^2\right]^{-1},\ 0 \le f_e \le 1,\ 0 \le f_m \le 1. \tag{59}$$

Thus, depending on the values of f_e and f_m, the denominator in Eq. 59 can approach zero and the maximum beam current can greatly exceed I_A.

3.6.5. *Beam Propagation in Plasma*
When a charged particle beam propagates through plasma, the plasma ions can neutralize the beam space charge. When this occurs, $E_r \to 0$ and, as a result, the beam constricts because of its self-consistent pinch field $B\phi$. For beam currents in excess of the Alfvén limiting current, B_ϕ is sufficient to reverse the direction of the beam electron trajectories at the outer layer of the beam. However, depending on the plasma conductivity σ, the induction electric field at the head of the beam [due to $dB/dt \sim dI/dt$ in Eq. 1] will produce a plasma current $I_p = -I_b$. Hence, the pinch field

$$B_\phi (r) = \frac{\mu_0}{2\pi r} [I_b (r) + I_p] \tag{60}$$

can vanish allowing the propagation of beam currents I_b in excess of I_A.

Because of the finite plasma conductivity, the current neutralization will eventually decay in a magnetic diffusion time τ_d given by Eq. 33. During this time a steady state condition exists in which no

net self-fields act on the beam particles. While in a steady state, beam propagation is limited only by the classic macro-instabilities such as the sausage instability and the hose (kink) instability.

When the beam undergoes a small displacement, the magnetic field lags behind for times of the order τ_d. This causes a restoring force to push the beam back to its original position, leading to the well-known $m = 1$ (for a $e^{im\phi}$ azimuthal dependency) kink instability.

3.6.6. *Beam Propagation Along an External Magnetic Field*
An axially directed guide field B_z produces an azimuthal current component I_ϕ through Eq. 2. This modification to the conducting current follows by balancing the energies

$$W_{\perp\ kin} - \frac{1}{2\mu_0} B_z^2 \pi a^2 - \frac{\mu_0}{8\pi} I^2 + \frac{1}{2} \varepsilon_0 E_r^2\,(a)\,\pi a^2 = 0 \tag{61}$$

In the absence of any background confining gas pressure $p(a)$, the maximum current is

$$I_{\max} = I_\phi \beta^2 \left[\beta^2 - (1 - f_e)^2\right]^{-1} \tag{62}$$

For the case of an axial guide field, the axial current I_z is not limited to I_A and depends only on the strength of the balancing I_z (B_z) current (magnetic field). In terms of the magnetic fields, the current flows as a beam when

$$B_z >> \frac{\left[(1 - f_e)^2 - \beta^2\right]^{1/2}}{\beta} \quad B_\phi \tag{63}$$

Note that Eq. 56 still holds; that is, a cylindrical conductor around the electron beam is necessary for the beam to propagate.

Equation 63 finds application in accelerators such as the high-current betatron [Hammer and Rostocker 1970]. In spite of the high degree of axial stabilization of a charged particle beam because of B_z, appreciable *azimuthal* destabilization and filamentation can occur because of the diocotron effect. This can be alleviated by bringing the metallic wall close to the beam.

3.6.7. *Schönherr Whirl Stabilization*
The transverse kinetic energy term $W_{\perp kin}$ in Eq. 35 explains an observation made long ago [Schönherr 1909]. High-current discharges conduct more current if the discharge is subject to an externally impressed rotation v_ϕ. This phenomena can also be expected in astronomical situations if the charged particle beam encounters a nonaxial component

of a magnetic field line that imparts a spin motion to the beam or if a gas enters transversely to an arc discharge-like plasma.

3.6.8. *The Carlqvist Relation*

An expression having broad applicability to cosmic plasmas, due to Carlqvist [1988], may be obtained from Eq. 35 if the beam is taken to be cylindrical and in a rotationless and steady-state condition:

$$\frac{\mu_0}{8\pi} I^2(a) + \frac{1}{2} G\bar{m}^2 N^2(a) = \Delta W_{B_z} + \Delta W_k \tag{64}$$

Thus, in a straightforward and elegant way, the gravitational force has been included in the familiar Bennett relation. Through Eq. 64, the Carlqvist Relation, the relative importance of the electromagnetic force and the gravitational force may be determined for any given cosmic plasma situation. This relation will now be applied to the two commonest pinch geometries–the cylindrical pinch and the sheet pinch.

3.6.9. *The Cylindrical Pinch*

Consider the case of a dark interstellar cloud of hydrogen molecules ($\bar{m} = 3 \times 10^{-27}$ kg and $T = T_i = T_e = T_n = 20$ K). Carlqvist (1988) has given a graphical representation of the solution to Eq. 64 for these values and this is shown in Figure 2 for discrete values of ΔW_{Bz}. Several physically different regions are identified in this figure.

The region in the upper left-hand part of the figure is where the pinching force due to I and the magnetic pressure force due to B_z constitute the dominating forces. Equation (2.52) in this region reduces to

$$\frac{\mu_0}{8\pi} I^2(a) \approx \Delta W_{B_z} \tag{65}$$

representing a state of almost force-free magnetic field.

Another important region is demarked by negative values of ΔW_B. In this region an outwardly directed kinetic pressure force is mainly balanced by an inwardly directed magnetic pressure force. Hence the total pressure is constant and Eq. 64 is approximately given by

$$NkT + \Delta W_{B_z} \approx 0 \tag{66}$$

For yet larger negative values of ΔW_B, the magnetic pressure force is neutralized by the gravitational force so that Eq. 64 reduces to

$$\frac{1}{2} G\bar{m}^2 N^2(a) \approx \Delta W_{B_z} \tag{67}$$

Another delineable region is where $\Delta W_B = 0$, where Eq. 64 reduces to the Bennett relation,

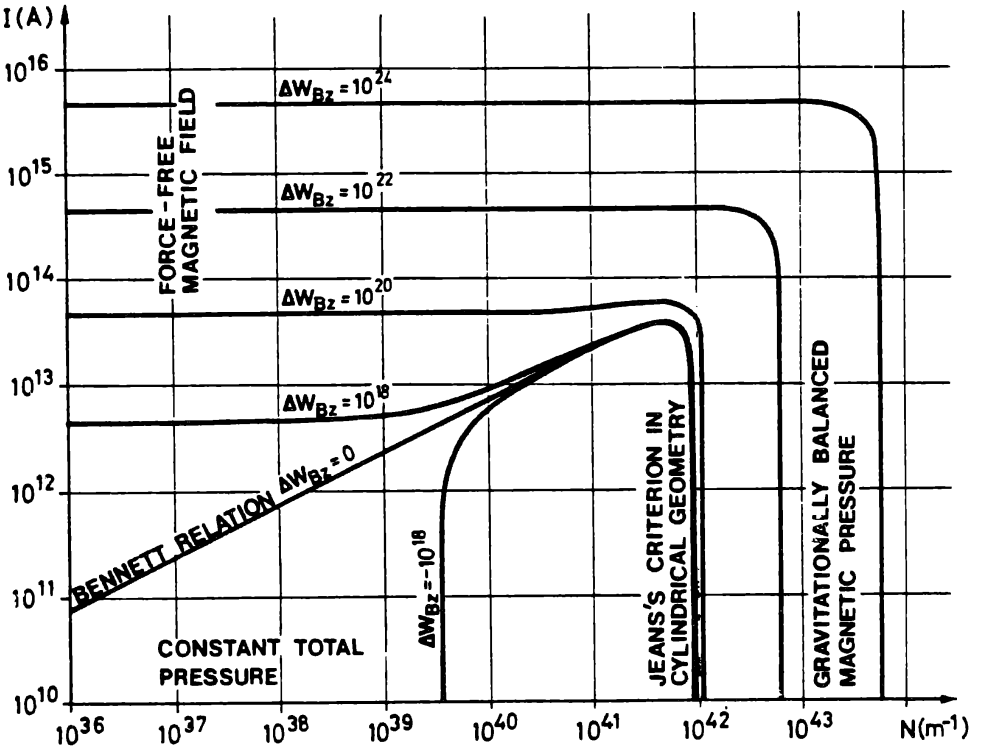

Figure 2. The total current I in a generalized Bennett pinch of cylindrical geometry as a function of the number of particles per unit length N. The temperature of the plasma is $T = 20$ K while the mean particle mass is $\bar{m} = 3 \times 10^{-27}$ kg. It is assumed that the plasma does not rotate ($\omega = 0$) and that the kinetic pressure is much smaller at the border of the pinch than in the inner parts. the parameter of the curves is ΔW_{Bz}, representing the excess magnetic energy per unit length of the pinch due to an axial magnetic field B_z (courtesy of P. Carlqvist).

$$\frac{\mu_0}{8\pi} I^2(a) \approx \Delta W_k(n, T) \tag{68}$$

Another region of some interest is where the classic Bennett relation line turns over into an almost vertical segment. Here, the pinching force of the current may be neglected, leaving the kinetic pressure force to balance only the gravitational force so that

$$\frac{1}{2} G \bar{m}^2 N^2(a) \approx NkT \tag{69}$$

This is the Jeans's criterion in a cylindrical geometry.

The size or radius of the cylindrical pinch depends on the balancing forces. For the Bennett pinch Eq. 68 the equilibrium radius is

$$a \approx \frac{I}{2\pi} \sqrt{\frac{\mu_0}{2nkT}} \tag{70}$$

Küppers (1973) has investigated the case of a REB propagating through plasma. Space charge neutralization ($E_r = 0$) is maintained when $n_e +$

$n_b = n_i$. For this case, the replacements $n \rightarrow n_b$ and $T \rightarrow T_b - T_e$ are made to $\Delta W_k\,(n, T)$, where T_b is the beam temperature and T_e is the background plasma electron temperature. For the space charge neutralized REB,

$$a \approx \frac{I_b}{2\pi}\sqrt{\frac{\mu_0}{2n_b k\,(T_b - T_e)}} \tag{71}$$

Note that physically acceptable solutions for the equilibrium radius are obtained only when the beam temperature (in the axial direction for a cold beam) exceeds the plasma electron temperature.

From Eq. 65, the equilibrium radius of a pinch balanced by an internal field B_z is

$$a \approx \frac{\mu_0 I}{2\pi B_z} \tag{72}$$

4. Radiation Characteristics of the Plasma State

Electromagnetic waves propagated in cosmic space derive from a variety of mechanisms. The major contribution in the optical region of the spectrum is from radiation resulting from bound-bound electron transitions between discrete atomic or molecular states, free-bound transitions during recombination, and free-free transitions in the continuum. In the latter case, when for transitions between levels, radiation classified as bremsstrahlung results from the acceleration of electrons traveling in the vicinity of the atom or ion.

In addition, there are other mechanisms of considerable importance operating in the radio region. In particular, there are noncoherent and coherent mechanisms connected with the existence of sufficiently dense plasmas which are responsible for radiation derived from plasma oscillations, such as the sporadic solar radio emissions. This radiation cannot be attributed to the motion of individual electrons in a vacuum but is due to the collective motion of electrons at the plasma frequency

$$\frac{\omega_{pe}}{2\pi} = \frac{1}{2\pi}\sqrt{\frac{n_e e^2}{m_e \varepsilon_0}} = 9\sqrt{n_e},\ \text{Hz} \tag{73}$$

for an electron density n_e (m^{-3}). This often occurs in cosmic plasma when electron beams propagate through a neutralizing plasma background.

4.1. Synchrotron Radiation

When a plasma is subjected to a magnetic field there is yet another mechanism which plays an extremely important role in radio astronomy. The frequency and angular distribution of the radiation from free electrons moving in the presence of a magnetic field undergoes dramatic changes as the electron energy is increased from nonrelativistic to extreme relativistic energies. Essentially three types of spectra are found. Names such as cyclotron emission and magnetobremsstrahlung are used to describe the emission from nonrelativistic and mildly relativistic electron energies, whereas the name synchrotron radiation is traditionally reserved for highly relativistic electrons because it was first observed in 1948 in electron synchrotrons.

Synchrotron radiation is characterized by a generation of frequencies appreciably higher than the cyclotron frequency of electrons (or positrons) in a magnetic field, a continuous spectra whose intensity decreases with frequency beyond a certain critical frequency, highly directed beam energies, and polarized electromagnetic wave vectors.

In astrophysics, nonthermal (nonequilibrium) cosmic radio emission is, in a majority of cases, synchrotron radiation. This is true for general galactic radio emission, radio emission from the envelopes of supernovae, and radio emission from double radio galaxies and quasars (continuum spectra). Synchrotron radiation also appears at times as sporadic radio emission from the sun, as well as from Jupiter. In addition, optical synchrotron radiation is observed in some instances (Crab nebula, the radiogalaxy and "jet" in M87-NGC 4486, M82, and others). This apparently is also related to the continuous optical spectrum sometimes observed in solar flares. Synchrotron radiation in the X ray region can also be expected in several cases, particularly from the Crab nebula.

When cosmic radio or optical emission has the characteristics of synchrotron radiation, a determination of the spectrum makes possible a calculation of the concentration and energy spectrum of the relativistic electrons in the emission sources. Therefore, the question of cosmic synchrotron radiation is closely connected with the physics and origin of cosmic rays and with gamma- and X ray astronomy.

Synchrotron radiation was first brought to the attention of astronomers by H. Alfvén; and N. Herlofson; [1950], a remarkable suggestion at a time when plasma and magnetic fields were thought to have little, if anything, to do in a cosmos filled with "island" universes (galaxies).[9] The recognition that this mechanism of radiation is important in astronomical sources has been one of the most fruitful developments in astro-

[9] The "island universes" concept was introduced by the philosopher Kant (1724-1804).

physics. For example, it has made possible the inference that high-energy particles exist in many types of astronomical objects, it has given additional evidence for the existence of extensive magnetic fields, and it has indicated that enormous amounts of energy may indeed be converted, stored, and released in cosmic plasma.

The polarization, spectral, temporal, power, and directivity properties of synchrotron radiation are well known [Peratt 1992].

4.1.1. *Directivity*

The gain, or directivity of the synchrotron radiation zone is given by

$$G\left(\beta_{||},\beta_{\perp},\theta\right)=\frac{3}{4}\left(1-\beta^2\right)F\left(\beta_{||},\beta_{\perp},\theta\right) \tag{74}$$

where

$$F\left(\beta_{||},\beta_{\perp},\theta\right)= \frac{4g_{||}^2\left[\left(1-\beta_{||}^2\right)\left(1-\cos^2\theta\right)-4\beta_{||}\cos\theta\right]-\left(1-\beta_{||}^2+3\beta_{\perp}^2\right)\beta_{\perp}^2\sin^4\theta}{4\left(g_{||}^2-\beta_{\perp}^2\sin^2\theta\right)^{7/2}} \tag{75}$$

where

$$\beta^2=\left(\frac{v_{||}}{c}\right)^2+\left(\frac{v_{\perp}}{c}\right)^2=\beta_{||}^2+\beta_{\perp}^2 \tag{76}$$

and $v_{||}$ and $v_{\perp}$ are the instantaneous particle velocities along and perpendicular to B_0, respectively.[10]

4.1.2. *Spectrum*

The total emission per unit radian frequency interval is

$$P_{\omega}^{T}=\frac{\sqrt{3}e^2\omega_b}{8\pi^2\varepsilon_0 c} \times\left\{\beta_0\left(1-\beta_0^2\right)\gamma^2\frac{\omega}{\omega_c}\left[2K_{2/3}\left(\frac{\omega}{\omega_c}\right)-\frac{\gamma^2\left(1-\beta_0^2\right)}{\beta_0^2}\int_{\omega/\omega_c}^{\infty}K_{1/3}\left(t\right)dt\right]\right\} \tag{77}$$

where, by definition,

$$\begin{aligned}\omega_c&=\tfrac{3}{2}\omega_{\gamma}\gamma^3=\tfrac{3}{2}\omega_b\gamma^2\\&=2.64\times10^7 B_{0\ gauss}\left(\frac{W_{keV}}{511keV}\right)\ rad/s\end{aligned} \tag{78}$$

[10] Noteworthy in $G(\theta)$ is the inversion of gain direction between the cases $\beta_{||}=0$ as $\beta_{\perp}$ increases and the essentially forward emission in the relativistic case when $\beta_{||}/\beta_{\perp}$ is large.

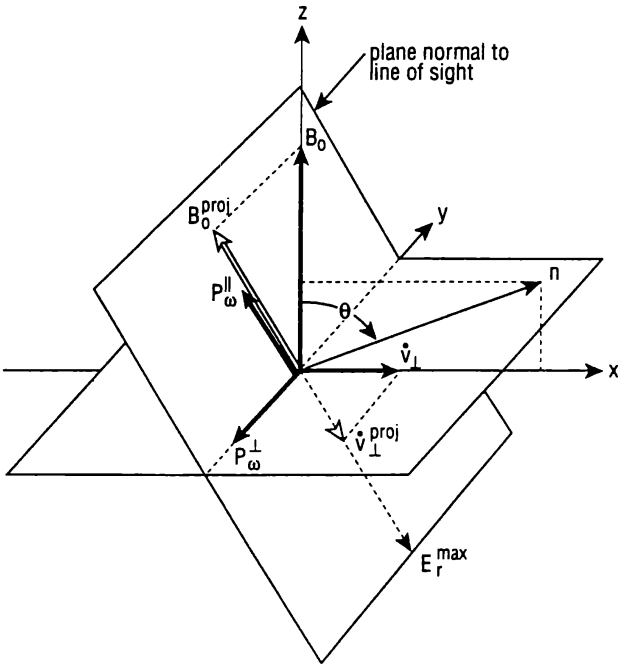

Figure 3. Orientation of the quantities $P_\omega^\perp$ and $P_\omega^{||}$.

4.1.3. *Polarization*

The power radiated into the mth harmonic may be written as the sum of two parts,

$$P_\omega(\omega, \beta, \theta) = P_\omega^{(1)} + P_\omega^{(2)} \tag{79}$$

where

$$P_\omega^{(1)}(\theta) = \frac{e^2\omega^2}{8\pi^2\varepsilon_0 c}\sum_1^\infty \left\{\frac{\cos\theta - \beta_{||}}{\sin\theta} J_m(x)\right\}^2 \delta(y) \tag{80}$$

$$P_\omega^{(2)}(\theta) = \frac{e^2\omega^2}{8\pi^2\varepsilon_0 c}\sum_1^\infty \{\beta_\perp J'_m(x)\}^2 \delta(y) \tag{81}$$

whose orthogonal field vectors $E_m^{(1)}$ and $E_m^{(2)}$ ($p_\omega \sim E_m^2$) lie parallel and perpendicular, respectively, to the projection of B_0 on the plane normal to the line of sight $\left[B_0^{\perp n} = B_0 - (B_0 \cdot n)\, n\right]$ as shown in Figure 3.[11] The easiest way to determine the polarization of the mth harmonic is to take the ratio of the field amplitudes in Eqs.(6.75) and (6.76),

$$R_m = -\frac{E_m^{(1)}}{E_m^{(2)}} = -\left(\frac{\cos\theta - \beta_{||}}{\beta_\perp \sin\theta}\right)\frac{J_m(\psi m)}{J'_m(\psi m)} \tag{82}$$

[11] While $P_\omega^{(0)}$ has no rotation, $P_\omega^{(1)}$ does rotate.

where $\psi = \beta_\perp \sin\theta / \left(1 - \beta_{||} \cos\theta\right)$. The parameter R_m defines the ellipticity of the propagating wave in the direction θ. When $|R_m| = 1$, the wave is circularly polarized while when $R_m = 0$, the wave is linearly polarized. When $0 < R_m < 1$, the wave is elliptically polarized in the ratio of the field amplitudes oriented along the minor and major axes of the ellipse. The polarization of the extraordinary mode rotates in the same sense as does the radiating electron.

4.2. Transition Radiation

Even in the absence of a magnetic field, astrophysical plasmas are capable of producing polarized radiation and large scale radiation patterns having diffraction-like patterns. At cellular interfaces delineating astrophysical plasmas of differing constituency, the passage of electrical currents can produce *transition radiation*, first studied by Frank and Ginzburg [1945]. Transition radiation is produced by the propagation of charged particles through the interface between media with differing dielectric constants. It is caused by a collective response of the matter surrounding the particle trajectory to readjust the electromagnetic field of the charged particle.

If for example, electrons pass through the highly conductive interface (e.g., a cell wall or sheet current) separating two relatively tenuous regions, an angular distribution of energy occurs, given by

$$W(\omega, \Theta) = \frac{e^2}{4\pi^3} \sqrt{\frac{\mu_0}{\varepsilon_0}} \beta^2 \frac{\sin^2 \Theta}{\left(1 - \beta^2 \cos^2 \Theta\right)^2} \tag{83}$$

where Θ is the angle between the electron trajectory and the emitted radiation. For relativistic electrons ($\beta \sim 1$) the emission is sharply peaked in the region of small Θ and is maximum when $\Theta \sim 1/\gamma$. In all cases, the transition radiation is totally polarized. The plane of polarization is given by the electron trajectory and the direction of observation.

If the path of an electron is unobstructed over a distance greater than the formation length

$$\Lambda = \frac{2c}{\omega\left(1 - \beta^2 + \Theta^2\right)} \tag{84}$$

then the angular distribution of Eq. 83 is small. If the free path d is smaller than Λ, the angular distribution is broadened by diffraction and the radiation is strongly suppressed below an angle of

$$\Theta_m \approx \sqrt{\frac{2c}{\omega d}} \tag{85}$$

Integrating Eq. 83 over Θ gives the spectral energy,

$$W(\omega) = \frac{e^2}{3\pi^3}\sqrt{\frac{\mu_0}{\varepsilon_0}}\left\{\frac{3}{8}\frac{\beta^2+1}{\beta^2}\ln\frac{1+\beta}{1-\beta} - \frac{3}{4\beta^2}\right\} \tag{86}$$

If the beam of electrons is bunched, the emitted radiation from different electrons adds coherently when the wavelength λ is comparable to or longer than the beam bunch. Thus the intensity is proportional to the number of electrons squared. Long a topic of theoretical interest, transition radiation has been experimentally verified in the far infrared [Happek et al. 1991].

Thus coherent transition radiation may given information about large scale cellular astrophysical transition regions.

4.3. Thermal Radiation

The spectral distribution of the radiation of a black body in thermodynamic equilibrium, for a single polarization, is given by the Planck formula

$$B_0(\omega, T) = \frac{\hbar\omega^3}{8\pi^3 c^2}\frac{1}{e^{\hbar\omega/kT}-1} \tag{87}$$

Non-black body radiation from plasma can be thermalized by filaments or even carbonaceous needles in space. The radiation intensity is

$$I_{\omega M} = S_\omega\left(1 - e^{-M\alpha_w L}\right) \tag{88}$$

Note that the radiation intensity increased for larger M because of each additional filament current source. The absorption coefficient at $\theta = \pi/2$ is [Trubnikov 1958, Peratt 1992]

$$\alpha_\omega = \frac{\omega_p^2}{\omega_b c}\sum \Phi_m\left(\omega/\omega_b\mu\right) \tag{89}$$

The quantities $\Phi_m = \Phi_m(\omega/\omega_b, \mu)$ are defined by

$$\Phi_m = \sqrt{2\pi}\frac{\mu^{5/2}}{(\omega/\omega_b)^4}m^2\sqrt{m^2-(\omega/\omega_b)^2}\,e^{-\mu[m(\omega/\omega_b)-1]}A\left[m/\left(\omega/\omega_b\right)\right] \tag{90}$$

where $\mu = m_0c^2/kT$. The quantities $A_m = A_m(\gamma)$ are given by

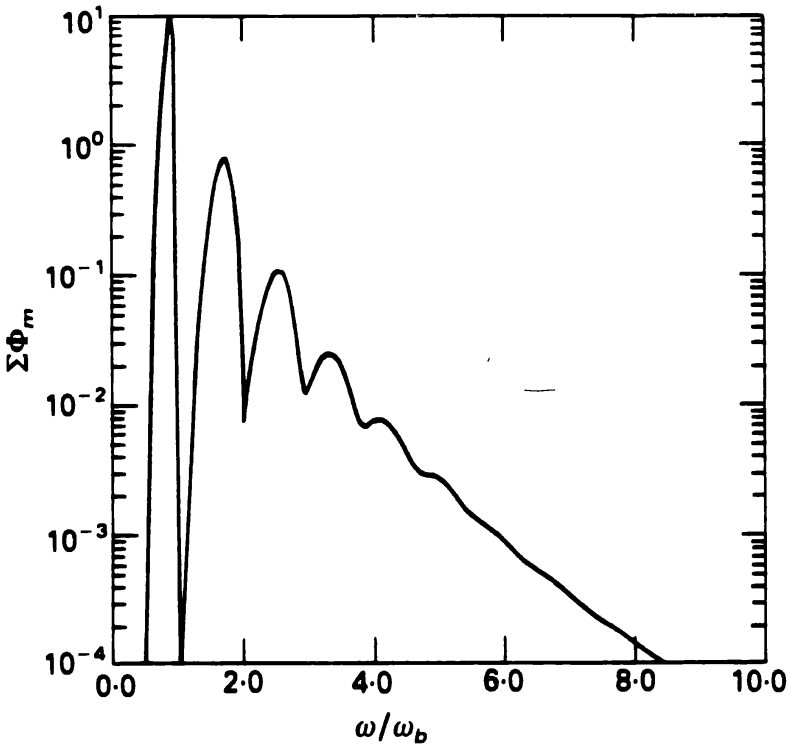

Figure 4. Calculated spectrum of radiation emitted by a plasma with electron temperature of 30 keV. Self-absorption effects are included.

$$A_m^{(X,O)}(\gamma) = \begin{cases} \frac{(m\beta)^{2m}}{(2m+1)!}\left[1; \frac{\beta^2}{2m+3}\right] & m\beta << 1 \\ \frac{e^{2m/\gamma}}{\sqrt{16\pi m^3\gamma}}\left(\frac{\gamma-1}{\gamma+1}\right)^m\left[1; \frac{\gamma(\gamma^2-1)}{2m}\right] & \gamma^3 << m \\ \frac{1}{4\sqrt{3}\pi m\gamma^2}\left[\int_{2m/3\gamma^3}^{\infty} K_{5/3}(t)\,dt \pm K_{2/3}(2m/3\gamma^3)\right] & \gamma, m >> 1 \end{cases} \tag{91}$$

The optical depth for M Birkeland currents is $\tau_\omega = \alpha_\omega ML$ or

$$\tau_\omega = \left(\frac{\omega_p^2 LM}{\omega_b c}\right)\sum_m \Phi_m \tag{92}$$

The spectral characteristics of the emission are contained in the function Φ. Figure 4 shows a plot of $\Sigma\Phi_m$ for the first one hundred harmonics as a function of ω/ω_b for $T = 30$ keV. This value is typical of the thermal temperatures in a plasma filament but is appreciably less than the energies of particles in a relativistic beam. Only the extraordinary wave is considered; the contributions from the ordinary wave are usually small.

The broadening of the individual lines is due to the relativistic change of mass. A given line contributes only to frequencies $\omega \leq m\omega_b$ with the highest energy electrons being responsible for the emission at

the lowest frequency. The smearing of the successive harmonics produces an almost monotonically decreasing spectrum at higher frequency. For $T = 30$ keV, $m \sim 5$ is the harmonic above which smearing prevails. To a fair approximation, the total intensity leaving the filaments is

$$I(\theta = \pi/2) \cong \int_0^{\omega^*} B_0(\omega, T)\, d\omega = \frac{\omega_b^3 kT}{24\pi^3 c^2} (m^*)^3 \tag{93}$$

where $m^* = \omega^*/\omega_b$ is the harmonic number beyond which the emission effectively ceases to be black-body. An empirical relation for m^* for mildly relativistic plasma has been derived by Trubnikov [1958]; and modified to the case of M filaments,

$$(m^*)^6 = 0.57 \left(\frac{20\omega_p^2}{3\omega_b c} \right) LMT \tag{94}$$

Equation 94 is valid under the approximation $mc^2 >> kT$.

5. Formulation for the Particle-in-Cell Simulation of Astrophysical Plasmas

The modern study of the numerical simulation of astrophysical and space plasma can be separated into two categories:

1. Magnetohydrodynamics, or the fluid-like behavior of plasma in the presence of magnetic fields.

2. Particle kinetics, or the discrete electron-ion behavior in self-consistent and external electromagnetic fields.

The first category, Magnetohydrodynamics, was invented by Alfvén to study instability mechanisms associated with the solar atmosphere. Alfvén felt that the magnetohydrodynamics approximation had to be treated with caution and instead favored the particle approach to problems in plasma physics.[12] Examples that require a particle treatment include cases where electric fields parallel to a magnetic field exist (a common occurance in astrophysical plasmas), double layers, critical ionization velocity mechanisms, transition radiation, and synchrotron

[12] For example, the concept of a 'frozen-in magnetic field' has no physical meaning in the presence of an axial electric field.

radiation. Likewise, Buneman suggested that the magnetohydrodynamic synthesis could be replaced entirely by the particle-in-cell methodology, once computer resources attained a capability for handling multimillions of particles and cells in tractable timescales. According to Buneman [1976]:

> "We may conclude from these preliminary results that a feasible full 3D, EM simulation can yield a lot of good physics. In particular, it can reproduce hydromagnetic phenomena (such as Alfvén waves) as well as typical plasma phenomena. In fact, particle simulation may eventually turn out to be the easiest method of doing hydromagnetics on the computer."

Dawson [1993] echoes this sentiment:

> "Magnetohydrodynamic models have existed since the beginning of plasma modeling. Over the years more complete fluid models have been developed that include resistivity, viscosity, heat conduction and other nonideal effects.
>
> Simple fluid models leave out the physics that is responsible for much of the important behavior of plasmas. they leave out kinetic effects, which contribute to damping and to nonlinear saturation of unstable modes and can drive instabilities. Such effects are probably at the heart of determining properties of plasma and heat transport across magnetic fields."

In fact, the numerical magnetohydrodynamic method has seen great use, especially in problems where the plasma is dense enough that collisions are frequent enough that the plasma is in local thermodynamic equilibrium. The approach has had great success in the modeling of inertially confined plasmas with sophisticated codes such as LASNEX.[13] Even though collisions are infrequent in a space plasma and it is far from equilibrium, MHD is used to model the interaction of the solar wind with the earth's magnetosphere and the dynamics of the solar corona [Brackbill 1987] as-well-as magnetic merging in astrophysical plasmas [Biskamp 1997].

[13] LASNEX is a two-dimensional, azimuthally symmetric Lagrangian code that is often used to model laser-matter interactions and plasma expansions (Zimmerman and Kruer, 1975). The equation of motion for the single fluid, which may consist of a composite of different materials, includes contributions to the pressure from ions, thermal and suprathermal electrons, radiation, magnetic fields, and ponderomotive effects. The nonlocal thermodynamic equilibrium atomic physics model includes a solution of the time–dependent ionization and radiation equations in an average atom approximation. Radiation is also treated by separate photon groups, with emission and transport calculated from a set of coupled flux-limited multigroup diffusion equations.

5.1. The Basic Laws of Plasma Physics

The numerical simulation by particles of plasma physics began in the 1950s by Dawson at Princeton and Buneman at Stanford, where various plasma phenomena were identified and studied. It should be mentioned that, in the beginning, it was not at all apparent that the technique developed to study pure electron beam propagation in microwave devices could be applied to the plasma state of matter. Unlike the cold electron beam with charges of all one sign, plasmas often consist of thermal distributions with essentially equal density of charges of opposite sign and greatly different masses. In studying cold electron beams, a few dozen particles sufficed to reproduce the essence of the experiment. However, in laboratory plasmas one has scale lengths greater then the Debye length ($L >> \lambda_D$) and the number of particles in a Debye cube $N_D \equiv n\lambda_D^3$ is much greater than one ($N_D >> 1$). For example, the earth's ionosphere has $N_D \approx 10^4$ and the literal simulation of it over its scale length appears infeasible. However the general character of plasmas can often be found by studying the *collective behavior of collisionless plasmas at wavelengths longer than the Debye length,* $\lambda \geq \lambda_D$. It was found that another characterization of a plasma is that (1) the thermal kinetic energy is much greater than the microscopic potential energy, and (2) the ratio of collision to plasma frequencies is much less than one. Both requirement can be met with rather low values of N_D [Birdsall and Langdon 1985]. Conditions 1 and 2 may be met for finite sized particles called clouds. Clouds occur naturally in simulations which use a spatial grid for interpolation, as well as in simulations which employ spectral methods where the particle profile (usually gaussian) is specified in **k** space.

The term "particle-in-cell" derives from Frank Harlow and his group's work at Los Alamos in the 1950s in investigating the fluid nature of matter at high densities and extreme temperatures. Modern descriptions of the particle-in-cell technique as related to plasma physics are found in the two texts *Computer Simulation Using Particles* [Hockney and Eastwood 1981] and *Plasma Physics via Computer Simulation* [Birdsall and Langdon 1985].

We begin our approach by stating the laws of plasma physics in more or less the form which it has been found convenient to program: the equation of motion for the particles with the Lorentz force Eq. 5, and the Maxwell laws for the electric and magnetic fields Eqs. 1- 4.

5.2. Multidimensional Particle-in-Cell Simulation

5.2.1. *Sampling Constraints in Multidimensional Particle Codes*

The particle-in-cell technique for the analysis of complex phenomena in science has evolved from 1D through $1\frac{1}{2}$D, $1\frac{2}{2}$D, 2D, $2\frac{1}{2}$D, to 3D particle simulations. While at first one has to face certain limitations of an analytic nature, ultimately the limits are set by data management problems the resolution of which depends critically on the available hardware.

A trivial reason for the increasing difficulty of higher dimensional particle simulations is their demand for substantially greater particle numbers. With each added dimension the number of sampling particles has to be multiplied by a certain factor.

This also applies to "half-dimensions." It is customary to denote the inclusion of extra velocity components by referring to them as "half-dimensions." Typically, a pure 1D simulation simulates the plasma as rigid sheet particles, all parallel to the $y-z$ plane, say, and moving in the x direction. It ignores y and z motions of the planes. A $1\frac{1}{2}$D simulation keeps a record of possible y motions, uniform within each plane. Then the x-ward Lorentz force in the presence of a z-directed magnetic field can be taken into account, as well as the y-wards Lorentz force due to x motions. In a $1\frac{2}{2}$D simulation, dz/dt would be recorded as well. In a $2\frac{1}{2}$D simulation, $x, y, dx/dt$, and dz/dt are tracked (but not z); the particles are rigid straight rods whose motion along their axis is taken into account. One-and-a-half dimensional and $1\frac{2}{2}$D simulations have recently found application in space plasma work, namely for simulating the critical ionization phenomenon.

It is reassuring that relatively few samples can often give very good statistics. In many applications the velocity distributions stay close to maxwellian and a modest factor (typically four) in the sample number may suffice to deal with an added half-dimension. One exploits the favorable feature of statistics when initializing thermal velocity distributions: each velocity component is made up as the sum of four random numbers (each uniformly random in a certain interval). The resulting distribution (the "four dice curve," or cubic spline) is almost indistinguishable from the Gaussian.

However, when incrementing by a full dimension, sampling requirements jump dramatically. It is easily checked that the statistical potential energy fluctuations in a granular plasma compete with thermal energies when the particles are spaced on the order of a Debye length apart. Such a plasma would be essentially collision dominated. One is mostly interested in collective effects, since fluid codes are adequate for collision-dominated phenomena. Obviously, one needs several par-

ticles per Debye length; again, a modest number suffices. Now, most of the interesting phenomena to be resolved by simulation are on the scale of many Debye lengths (hundreds or thousands). Therefore, the addition of each full dimension calls for an increase of the number of particles by, typically, two orders of magnitude. In 1990 a 1D (electrostatic) simulation could barely be squeezed onto a personal computer, a 2D simulation called for a minicomputer or workstation, and a 3D simulation needed a supercomputer[14]. By the mid 1990's, rudimentary 3D simulations became possible on laptop computers.

5.2.2. *Discretization in Time and Space*

One-dimensional, $1\frac{1}{2}$D, and $1\frac{2}{2}$D simulations can be done without discretizing in space. The electrical interaction of sheets is independent of distance and one only needs to order the sheets to calculate their accelerations. Even if the sheets are of finite thickness or if they are "soft" (i.e., they have a smooth density profile across), only a few operations per sheet are needed to move them one time step. This is an effort of order N where N is the number of sheets.

However, in all simulations, time must be discretized. By studying the simulation of a simple 1D problem, namely, electrostatic oscillations in a cold plasma, and by Fourier transforming one's numerical procedure in time, one finds that while a time step $\delta t = \omega_p^{-1}$ yields the plasma frequency to 5% accuracy, for $\delta t > 2\omega_p^{-1}$ one runs into an instability.

To get over this severe limitation of the speed of simulation in cases where the phenomena of interest are much slower than electrostatic oscillations (typically ion responses), one can either use implicit methods, or one can make one's ions lighter than real ions. Much has been learned from simulations with ion-electron mass ratios as low as 16:1.

The big analytical problems in simulation arise when one advances to two dimensions. Interactions between rods of charge depend on distance, and the many remote rods are as important as the few near ones. For N rods, one has to calculate N^2 interactions and N itself might be typically two orders of magnitude larger than for a 1D simulation.

In order to get back to an effort of order N per step in the particle advance, one tabulates the field over a spatial grid and calculates the self-consistent field from a grid record of the charge and current-densities that each particle contributes.

[14] The approximate relationship of supercomputer performance and performance of those in other categories can be shown proportionately. If the performance of contemporary supercomputers is assigned a value of 100, the values in proportion to supercomputers are: minicomputers 0.1 to 5, workstation 0.1 to 1.0, and personal computers 0.001 to 0.1.

The permissible coarseness of the grid mesh becomes a critical issue and the problem of integrating the finite difference version (now in both space and time) of the field equation is far from trivial. Fortunately, both these subjects have been advanced to a state of relative completion and are exhaustively covered in two texts.

Very briefly and broadly, one can state that the grid should be fine enough to resolve a Debye length, and that smoothing or filtering of high spatial frequencies should be practiced in order to minimize "aliasing." This is the stroboscopic phenomenon of high frequencies parading as low frequencies (long wavelengths). Many physical instabilities set in preferentially at long wavelengths and can thus be excited numerically through aliasing. Grid effects can often be studied and checked in 1D where grids are optional. Smoothing can be achieved by particle shaping (i.e., spreading point particles into soft balls with a smooth bell-shaped internal density profile). Likewise, splines and finite-element techniques help.

Regarding the field update from the charge-current record, fast non-iterative methods for solving Poisson's equation over an L-by-M mesh have been developed. These include cyclic reduction in rows and columns, or Fourier transforming in one of the two dimensions (say, that of M). This is an effort to the order $LM \log_2 M$. Two-dimensional simulations go back historically to Hartree who initiated the simulation of the pure electron plasma which circulates in the magnetron. Hartree; also pioneered the time-centered update of the particles from Lorentz's equation Eq. 5

$$\frac{d\mathbf{v}}{dt} \pm \frac{e\mathbf{B}}{m} \times \mathbf{v} = \pm \frac{e\mathbf{E}}{m} \tag{95}$$

using $(v^{new} + vold)/2$ in the second (Lorentz) term and solving the linear equation for v^{new} explicitly. No limitation of $\omega_b \delta t = (eB/M)\,\delta t$ arises from this method except that for large values of $\omega_b \delta t$ the phases of the gyromotion are misrepresented. For small $\omega_b \delta t$ one gets the same results as with cycloid fitting, i.e., joining solutions of the type

$$\mathbf{v}^{\perp} = \mathbf{E} \times \mathbf{B}/B^2 + gyration\ at\ frequency\ \omega_b \tag{96}$$

for the components of the velocity transverse to $\mathbf{B}$. As regards this particle update, there is no significant increase in effort when advancing from $1\frac{1}{2}$ to 2D and 3D.

A further time-step limitation is encountered when one wants to integrate the full electromagnetic equations over the grid. Because Maxwell's equations (not including Poissons's) are hyperbolic (i.e., they contain a natural $\partial/\partial t$ or "update" term), they can be solved in an effort which is of the order of magnitude of the number of grid points,

LM in the 2D example discussed earlier. Essentially, one solves a wave equation. However, this process becomes unstable unless one observes the Courant speed limit $\delta t < \delta x/c$ in 1D, $\delta t < \delta x/c\sqrt{2}$ in 2D, and $\delta t < \delta x/c\sqrt{3}$ in 3D for square and cubic meshes of side δx. In many applications, scales chosen from other considerations are such that c is a large number and this restriction of δt results in a severe slowdown.

5.2.3. *Spectral Methods and Interpolation*

The Courant condition can be overcome by doing the entire field update in the transform domain. The Maxwell-Hertz-Heaviside laws for the electric and magnetic fields Eqs. 1- 4 can be conveniently combined into one equation for the complex field vector $\mathbf{F} = \mathbf{D} + i\mathbf{H}/c$. When Fourier transforming, this equation becomes

$$\frac{d\mathbf{F}}{dt} - c\mathbf{k} \times \mathbf{F} = -\mathbf{j} \tag{97}$$

for the spatial harmonic which goes like $(\exp i\mathbf{k} \cdot \mathbf{r})$. This field equation is surprisingly similar to that for the particle velocities Eq. 95 and has the corresponding solution for the transverse part of $\mathbf{F}$:

$$\mathbf{F}^{\perp} = \mathbf{j} \times \mathbf{k}/k^2 \ (\textit{magnetostatic field}) + \textit{circularly polarized wave rotating at angular frequency } ck \tag{98}$$

The time intervals at which one joins successive solutions of this form are dictated by the rate at which $\mathbf{j}$ changes, not by the magnitude of $c\mathbf{k}$.[15]

To Eq. 95 we should add an initial condition, namely, Poisson's

$$i\mathbf{k} \cdot \mathbf{F}_k = \rho_k \tag{99}$$

Fourier transforming all field-like quantities has many advantages. For instance, the longitudinal part of $\mathbf{F}$ (which is just $\mathbf{D}$) can be obtained from Poisson's equation as $\mathbf{k}\rho/k^2$. Of course, transforming in two dimensions rather than only one (as in the fastest Poisson solvers) makes for an effort of the order $LM\,(\log_2 L + \log_2 M)$. On the other hand, the ready availability of well-programmed FFTs and the additional benefits of spectral methods make up for this increase in effort.

In the transform domain one can perform the filtering, the particle shaping, an optimization for the spline fitting process, and the truncation of the interaction to be discussed in the section on boundary conditions. One does not have to use any spatial finite difference calculus for the field equations. However, a grid is still necessary since we

[15] The wavevector $k = \pi/\delta x, \pi\sqrt{(2)}/\delta x,$ or $\pi\sqrt{(3)}/\delta x$, according to the number of dimensions.

have only *discrete* numerical Fourier transforms between **r** space and **k** space.

This leaves the problem of interpolation in the mesh. By using high-order interpolation, one can greatly reduce aliasing and improve accuracy. Quadratic and cubic splines have been used, but this soon becomes expensive.[16] Linear interpolation is most commonly used. Interpolation is also needed when the particles contribute their charge and current to the $\rho, \mathbf{j}$ arrays.

Linear interpolation is then, in 2D, equivalent to "area weighting". For 3D, we have cut down the data look-up (or deposit) effort for linear interpolation by using a tetrahedral mesh. Each particle references only the four nearest mesh-point data. The tetrahedra result from drawing the space diagonals into a cubic mesh and introducing cubic center data. Interpolation of currents must be done twice in each step of each practice, once at its old position and once at its new position, since the current is that due to the movement between the two.

5.3. Techniques for Solution

The crucial equations, Eqs. 1 and 2, are in the "update" form, ideally suited to computers which are themselves devices whose function it is to update the state of their memory continually, albeit not continuously. If the time interval δt between updates is so chosen that during this interval changes of **E** and **B**, as seen by any particle, can be ignored in Eq. 1 and changes of **j** can be ignored in Eq. 2, each equation can be solved exactly for the entire interval no matter how long this interval is: The Lorentz equation Eq. 5 then produces cycloidal motion in a plane perpendicular to **B**, composed of a drift and a gyration Eq. 96. This may be accompanied by free fall parallel to **B**, generated by a parallel electric field component. Given the initial velocity and position, or given the position and displacement during the preceding time interval, the displacement during any subsequent interval, and the new position, can be computed precisely.

5.3.1. *Leap-Frogging Particles Against Fields*

The average value of the fields **E** and **B** for Eq. 95 or the current **j** to be used in Eq. 97 is taken to be the actual value at the middle of the time interval. Figure 5 shows how the updating from average values proceeds at equal intervals along a time axis. This involves the following:

[16] In a 3D, EM code, cubic splines would require each particle to look up 384 data to interpolate the **E** and the **B** that acts on it!

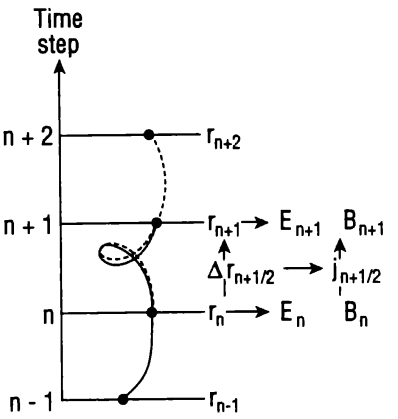

Figure 5. Leap-frogging particles and fields: At time n, cycloids with drifts and gyrations due to $\mathbf{E}_n$ and $\mathbf{B}_n$ are fitted through r_n and r_{n-1}, to be continued through r_{n+1}. Displacements Δr_{n+1} determine currents $\mathbf{j}_{n+1/2}$ from which the transverse fields $\mathbf{E}_n$, $\mathbf{B}_n$ are advanced to $\mathbf{E}_{n+1}$, $\mathbf{B}_{n+1}$. The longitudinal $\mathbf{E}_{n+1}$ is obtained from the r_{n+1}. Then, at time $n+1$, new cycloids (dotted) with drifts and gyrations due to $\mathbf{E}_{n+1}$ and $\mathbf{B}_{n+1}$ are fitted through r_{n+1} and r_n, to be continued through r_{n+2}, etc.

1. Construct the cycloidal orbit of a particle from t_{n-1} through t_n to t_{n+1} using the known mean values of $\mathbf{E}_n$ and $\mathbf{B}_n$ at t_n (the middle of the interval) and the known particle positions at t_{n-1} and t_n.

2. This gives the displacement of the particles from t_n to t_{n+1}, and their final positions at t_{n+1}.

3. The harmonic $\mathbf{j}_k$ of the mean current flowing during the last interval is obtained by summing all the displacements $\delta\mathbf{r}$ with phase factors $\exp i\mathbf{k}\cdot\mathbf{r}$ given by their mean positions, times $q/\delta t$.

4. The transverse fields $\mathbf{F}_k$ are now advanced by $\dot{\mathbf{j}}_k$ Eq. 97 from t_n to t_{n+1}.

5. The longitudinal fields $\mathbf{F}_k$ are obtained from ρ_k at t_{n+1} by summing with the new positions $\mathbf{r}$ at t_{n+1}.

6. The process is repeated from t_n through t_{n+1} and then to t_{n+2}.

Each time interval is covered by two cycloids for each particle, one with drift and gyrofrequency as given by the fields at the beginning of the interval, the other as given by the fields at the end of the interval. Both cycloids pass through the same points at the termini Figure 5.

5.3.2. *Particle Advance Algorithm*

The time interval δt must be smaller than $\sim \omega_p^{-1}$ for proper resolution of electrostatic plasma oscillations, and $\omega_b \delta t \leq 1$ to account for

synchrotron radiation or for ∇B drifts. The interpretation and implementation of this is as an electric acceleration followed by a magnetic rotation and another acceleration. The updating of the particle positions and velocities is done using a time-centered second-order scheme, valid for relativistic particle velocities,

$$\frac{v_{new} - v_{old}}{\delta t} = \frac{q}{\gamma m_0}\left[E + \left(\frac{v_{new} + v_{old}}{2}\right) \times B\right] \tag{100}$$

with the scaling[17]

$$E \leftarrow \frac{q\delta t}{2m_0}E, \; B \leftarrow \frac{q\delta t}{2m_0}B, \tag{101}$$

Eq. 100 is solved by the following sequence[18],

$$\begin{aligned}
\gamma_1 &= \left(1 - v^2/c^2\right)^{-1/2} \\
u_1 &= \gamma_1 v_{old} \\
u_2 &= u_1 + E \;\; (first\ half\ of\ electric\ acceleration) \\
\gamma_2 &= \left(1 + u_2^2/c^2\right)^{+1/2} \\
u_3 &= u_2 + \left(\frac{2}{\gamma_2^2 + B^2}\right)(\gamma_2 u_2 + u_2 \times B) \times B \\
u_4 &= u_3 + E \;\; (second\ half\ of\ electric\ acceleration)
\end{aligned}$$

$$\begin{aligned}
v_{new} &= u_4\left[1 + (u_4/c)^2\right]^{+1/2} \\
x_{new} &= x_{old} + \delta t v_{new}
\end{aligned} \tag{102}$$

This process is equivalent to rotating the deviation from the gyrocenter drift through the angle $2\arctan(qB\delta t/2m)$ –the "cycloid fitting"– combined with uninhibited electric acceleration along the magnetic field. It is second-order and time reversible.

Since this algorithm now properly accounts for the effects of relativity, particles are automatically restrained from exceeding the speed of light and need not be artificially braked at c. This limit on the distance traveled by a particle during a single time step plays an important role in particle data management.

---

[17] **E** describes half the electric acceleration and the magnitude of **B** is half the magnetic rotation angle during the time step.

[18] The sequence is mathematically concise when $\gamma = 1$. The quantity u is velocity in the sense of momentum per unit restmass. The relativistic γ is obtained from it as the square root of $1 + (u/c)^2$. The equation for u_3 is executed by first dividing B by γ^2 and then using "1" in place of γ^2. This accounts for the m rather than m_0 in the angle.

5.3.3. *Field Advance Algorithm*

The advance of the fields through one time step of arbitrary length (subject to $\mathbf{j}_k$ = constant) is mathematically just like that of the particles. According to Eq. 98, $\mathbf{F}_k$ consists of a constant component plus a rotating component. The constant part represents the magnetostatic field generated by the currents; the rotating part represents a circularly polarized electromagnetic wave. Again, the advance through any time interval δt is straightforward. The longitudinal (purely electric) component of the field is updated from the record of ρ at the end of the time step using Eq. 99.

We note, so far, we have not invoked finite difference calculus either in the space or time domain and, typically, the advance of the fields from Maxwell's equations is not restricted by any "Courant condition." However, δt is constrained by the fact that $\mathbf{E}$ and $\mathbf{B}$ should not change across the range of the orbit excursions during δt.

Equation 97 is used to trace the evolution of the transverse field only. The longitudinal, electrostatic field is constructed "from scratch" at the new time, using the charge density records:

$$F_k^{e-s} = ik\rho_k/k^2 \tag{103}$$

The longitudinal field, then, need not be held over through the particle move phase: it can be generated directly by Fourier transforming the charges accumulated during that phase. The transverse field is calculated as follows. A particular solution is constructed from $\mathbf{j}_k$ using

$$F_k^{m-s} = k \times j_k/k^2 \tag{104}$$

To $\mathbf{F}_k^{m-s}$ one has to add the rotating "electromagnetic" component

$$F_k^{e-m}(new) = F_k^{e-m}(old)\cos k\delta t - (k/k) \times F_k^{e-m}(old)\sin k\delta t \tag{105}$$

The new fields are then reconstructed from the updated pieces according to

$$F_k(new) = F_k^{m-s} + F_k^{e-m}(new) + F_k^{e-s} \tag{106}$$

and this is kept on record for the next field update.

The field seen by a particle must then be obtained by summation over the entire available spectrum

$$\begin{aligned} F(r) = D(r) + iH(r)/c &= (2\pi)^{-3}\int_k F_k e^{-ik\cdot r}dk \\ &= (2\pi)^{-3}\sum_{k_x}\sum_{k_y}\sum_{k_z} F_k e^{-ik\cdot r} \end{aligned} \tag{107}$$

To calculate **F**, we must introduce a grid over which field values are generated from the spectrum by FFTs, and we must interpolate the local field from the grid record. Likewise, charge and current harmonics must be built up by interpolation into a grid and subsequent FFTs.

Having avoided spatial grids and spatial finite-difference calculus so far, the introduction of a grid to obtain the electromagnetic fields from the spectrum F_k leads to difficulties associated with grids: inaccuracies and stroboscopic effects. These problems are reduced using higher-order interpolation methods [Buneman et al. 1980].

5.4. Issues in Simulating Cosmic Phenomena

5.4.1. *Boundary Conditions*

A major problem in space applications is to simulate free-space conditions outside the computer domain. Complex Fourier methods [with $\exp(i\mathbf{k}\cdot\mathbf{r})$] imply periodic repeats of the computed domain in all dimensions. If the simulation is to represent phenomena in a rather larger plasma, such repeats are acceptable, but for an isolated plasma of limited extent they become unrealistic. This problem can be overcome by keeping a generous empty buffer zone around the domain containing particles and truncating the interaction between charges beyond a certain radius so that the nonphysical repeats introduced by the Fourier method cannot influence the central plasma. This was first applied to gravitational simulations.

The most elusive boundary problem for space plasmas is the radiation condition. To decide what part of the field in the charge-current-free space outside the plasma is outgoing and what is incoming presents no problem in 1D and the incoming part can be suppressed.

In 2D the decision is more difficult. It requires information not only in the source-free boundary layer at any time but also over its past history. It almost seems as if, in principle, the entire past history is needed for the decision. However, Lindman found that a fairly short history (such as three past time steps) of the boundary suffices for an algorithm which will suppress all but 1% of the incoming radiation at all but the shallowest angles of incidence. However, just carrying an absorption layer in an outer envelope seems quite successful. This method simply multiplies the electric and magnetic field by a factor which smoothly approaches zero away from the plasma.

5.4.2. *Relativity*

A reason for keeping the mass coupled with the velocities in the update steps is that under relativistic conditions one really updates momenta rather than velocities. Note, however, that in the $qB\delta t/2m$ terms one

needs $m^{-1} = (m_0^2 + p^2/c^2)^{-1}$ where $p = mv$. During the rotation, this magnitude of the momentum does not change, but in the electric acceleration it does. After the full update of momenta, one must again divide by m in order to get $\mathbf{v} = \delta\mathbf{r}/\delta t$. In practice, v rather than the momentum is stored for each particle which means that at the beginning of the update one must calculate $m = m_0(1 - \beta^2)^{-1/2}$. Thus, there are three separate calls to a reciprocal square root in the relativistic advance of each particle. As system supplied square roots are time consuming and more accurate than needed for particle pushing, a Padé-type rational first approximation, followed by a Newton iteration, is used instead.

5.4.3. *Compression of Time Scales*

The number of steps required to simulate a significant epoch in the evolution of a real plasma configuration would be many million, typically, if t has to be of the order ω_p^{-1} or ω_b^{-1}. In order to bring this down to the more acceptable range of several thousand steps, one must compress the time scales. Compressing time scales can be achieved by (1) decreasing the ions' rest mass in relation to the electrons' rest mass, and (2) increasing temperatures so that typical particle velocities get closer to the velocity of light.

For an ion (proton) to electron simulation mass ratio of 16, ion gyrofrequencies $\omega_{bi} = eB/m_i$ will be high by a factor of $1836/16 = 115$, ion plasma frequencies $\omega_{pi} = \sqrt{n_i Z^2 e^2/m_i \varepsilon_0}$, ion thermal velocities $v_{Ti} = \sqrt{kT_i/m_i}$, the Alfvén velocity $v_A = \sqrt{B^2/\mu_0 n_i m_i}$, and the relative velocity in Biot-Savart attraction $v = I_z\sqrt{\mu_0 L/2\pi \sum m_i}$ will be high by factor of $\sqrt{1836/16} = 10.7$.

The exaggeration of temperatures provides one of several motivations for incorporating relativity into our codes. Note, incidentally, that even a 10-kV electron, a temperature typical of many space plasmas, already moves at $1/5$ c.

The exaggeration of "temperatures" of beam or current electrons can also be achieved by exaggerating the external electric field E_z responsible for accelerating the particles. This technique greatly reduces the number of time steps required to study a phenomenon such as Birkeland current formation and interaction in cosmic plasma. Since the current density is proportional to the electric field (i.e., $j_z = I_z/A = n_e e v_z \sim (n_e e^2/m_e)\, E_z t$), both the time required for the pinch condition Eq. 9 to be satisfied, and the relative velocity between parallel currents, are linearly related to E_z.

Of course, when economy necessitates time compression, the timescales must be "unfolded" upon simulation completion.

5.4.4. *Collisions*

Just as in real plasmas, there are encounters between particles and these give rise to collisional effects which influence the physics of the model. Since computer models are limited to some 10^6 particles whereas a laboratory plasma may have $10^{18} - 10^{20}$ particles and a galaxy, 10^{65} particles, each particle in the model is a "superparticle" representing many plasma electrons or ions. Thus the forces between model particles are much larger than in a real plasma and the collisional effects are much greater. Fortunately there is a way to reduce the model collisions to rates comparable with real plasmas. This involves the finite-size particle method [Birdsall and Langdon 1985].

Here we use a gaussian profile for particles. The shaping is done in **k**-space. This is achieved by first building up ρ_k and $\mathbf{j}_k$ for $|k| < k_{\max}$ (truncation of harmonics at maximum k), as if each computer particle were a point and then applying a gaussian filter in k-space [Buneman et al. 1980]. The particle shape is then of the form $\exp\left(-r^2 k_p^2/2\right)$, where the particle profile factor k_p is left as a users option: many simulations have used a profile which keeps the spectrum flat up to a fairly large k and then makes a rapid but smooth slope-off to zero at some desired k_{max}.

A limit to the maximum acceptable radius of the finite-sized particles is set by the collective properties of the plasma. If the effective radius of a gaussian particle is increased much beyond the Debye length, it takes over the role of the Debye length, causing collective effects to be altered.

In simulating a physical system, plasma or gravitating, it is usually sufficient to determine if the system models a collisionless one over the simulation time span. Experimental determination of the effective collisional frequency ν_c in 2D models closely follows the empirical law [Hockney and Eastwood 1981]

$$\frac{\nu_c}{\omega_p/2\pi} = N_D^{-1}\left[1 + \left(\frac{w}{\lambda_D}\right)^2\right]^{-1}$$

where w is the width of the particle and $N_D = n\lambda_D^2$ is the number of particles in a Debye square. In 3D simulations, the reduction of ν_c is achieved, without increasing N_D, by "softening the blow" of collisions–making the particles into fuzzy balls. Values of $\nu_c/\omega_p \approx 10^{-3}$ for gaussian profile particles for N_D of order unity have been calculated. This value is consistent with most plasmas, in laboratories or space.

So far we have only considered collisions between particle species that are charged. However, in weakly ionized plasmas where the number of uncharged particles may be hundreds or thousands of times more

prevalent, it is often the collision between the massive ions and the massive neutral atoms that cause a redistribution of energy, and concomitant effects, such as plasma heating. Collisions in weakly ionized plasmas have been successfully treated by melding PIC algorithms with MCC–Monte Carlo Collision–algorithms.

PIC codes involve deterministic classical mechanics which generally move all particles simultaneously using the same time step. The only part left to chance is usually limited to choosing initial velocities and positions and injected velocities. The objective for highly-ionized space plasma is usually seeking collective effects due to self and applied fields. On the other hand, MCC codes are basically probabilistic in nature, seeking mostly collision effects in relatively weak fields. For example, let a given charged particle be known by its kinetic energy W_{kin} and its velocity relative to some target particles. This information produces a collision frequency $\nu_{coll} = n_{target}\sigma W_{kin} v_{relative}$ and a probability that a collision will occur. This information is then used to describe electron collisions with neutrals (elastic scattering, excitation, and ionization) and ion collisions with neutrals (scattering and charge exchange).

The method is to use only the time step of the PIC field solver and mover, δt, and then to collide as many particles as is probable P in that δt separately. The actual fraction of particles in collision is $P = 1 - \exp(-\nu_{coll}\delta t)$. Note that we have slipped into treating our computer particles as single electrons, not as superparticles; the implication is that with a sufficient number of collisions, the resultant scatter in energy and velocity will resemble that of the single particles.

The end result of current efforts at including collisions in PIC codes due to Monte Carlo methods is the change in velocities of the particles. Thus, the only change from a collisionless run is that the particle velocities are varied in a time step. The last task at the end of a time step is to determine the new (scattered) velocity, and new particle velocities if ionization occurs (if ionization and/or recombination processes have been included in the MCC model). Each process is handled separately. Elastic collisions change the velocity angles of the scattered electrons; charge exchanges decrease ion energy and change velocity angles; ionizations do these and create an ion-electron pair, with new velocities. The effect on the neutral gas is not calculated because the lifetimes of the excited atoms are generally less than a time step.

When recombination rates are high, and if the source of energy to the plasma is terminated, gravitational effects must soon be included in the particle kinematics.

5.5. Gravitation

The transition of plasma into stars involves the formation of dusty plasma, the sedimentation of the dust into grains, the formation of stellesimals, and then the collapse into a stellar state [Alfvén and Carlqvist 197 8]. While the above process appears amenable to particle simulation, a crude approximation of proceeding directly from charged particles (actually a cloud of charged particles) to mass particles is made. The transition of charge particles to mass particles involves the force constant, that is, the ratio of the coulomb electrostatic force between two charges q separated a distance r,

$$F_q(r) = \frac{q^2}{4\pi\varepsilon_0 r^2} \tag{108}$$

to the gravitational force between two masses m separated a distance r,

$$F_G(r) = -\frac{Gm^2}{r^2} \tag{109}$$

In the particle algorithm this change is effected by the following:

1. Changing all particles to a single species.
2. Limiting the axial extent of the simulation to be of the order of less than the extent or the radial dimension (i.e., about the size of the expected double layer dimension).
3. Setting the axial velocities to zero.
4. Setting the charge-to-mass ratio equal to the negative of the square-root of the gravitational constant ($\times 4\pi\epsilon_0$).

This last change produces attractive mass particles via the transformation $\varphi_G(r) = \varphi_q(r)$ in the force equation $F = -\nabla\varphi$, where

$$\varphi_q(r) = -\frac{q^2}{4\pi\varepsilon_0 r} \tag{110}$$

and

$$\varphi_G(r) = -\frac{Gm^2}{r} \tag{111}$$

are the electrostatic and gravitation potentials, respectively.

5.6. Scaling Laws

The scaling of plasma physics on cosmical and laboratory scales generally involves estimates of the diffusion in plasma, inertia forces acting on the currents, the Coriolis force, the gravitational force, the centrifugal force, and the $\mathbf{j} \times \mathbf{B}$ electromagnetic force.

Specification of plasma density, geometry, temperature, magnetic field strength, acceleration field, and dimension set the initial conditions for simulation. The parameters that delineate the physical characteristics of a current-carrying plasma are the electron drift velocity

$$\beta_z = \frac{v_z}{c} \tag{112}$$

the plasma thermal velocity

$$\beta_{th} = \frac{v_{th}}{c} = \frac{(\lambda_D/\Delta)(\omega_p \delta t)}{c\delta t/\Delta} \tag{113}$$

and the thermal/magnetic pressure ratio

$$\beta_p = \frac{n_e k T_e + n_i k T_i}{B^2/2\mu_0} = \frac{(\lambda_D/\Delta)^2 (\omega_p \delta t)^2 \, 4\,(1 + T_i/T_e)}{(c\delta t/\Delta)^2 (\omega_{c0}/\omega_p)^2} \tag{114}$$

The parameter δt is the simulation time step, Δ is the cell size, and c is the speed of light. All dimensions are normalized to Δ and all times are normalized to δt. The simulation spatial and temporal dimensions can be changed via the transformation

$$\frac{c\delta t}{\Delta} = \frac{c\delta t'}{\Delta'} = 1 \tag{115}$$

where $\Delta' = \alpha\Delta$ and $\delta t' = \alpha \delta t$, for the size/time multiplication factor α. The values of n, T, B, and E remain the same regardless of whether the simulations are scaled to Δ and δt or to Δ' and $\delta t'$.

One immediate consequence of the rescaling is that, while the dimensionless simulation parameters remain untouched, the resolution is reduced, that is,

$$\omega \delta t = \omega' \delta t' \tag{116}$$

where $\omega' = \omega/\alpha$ rad s^{-1} is the highest frequency resolvable.

To convert simulation results to dimensional form, it is sufficient to fix the value of one physical quantity (e.g., B_ϕ).

5.7. Three Dimensionality

As in laboratory plasmas, astrophysical and space plasmas are three dimensional in nature even if their source is symmetrically two-dimensional. Lindberg [1978] found that full physics models and approximations were of secondary importance to a three dimensional spatial description in benchmarking observations of a charged particle beam flowing along a curved magnetic field. The problem is now known as the *Reverse Deflection Problem.*

The Reverse Deflection Problem is a relatively simple experimental setup consisting of a plasma gun source with external coil magnets arranged to produce a curved magnetic field. The plasma gun is energized and charged particles are emitted into an initially linear magnetic 'guide' field. However, as the beam encountered the bend in the field, all *a priori* theoretical predictions and two dimensional simulations of the beam kinetics were incorrect (Figure 6). Furthermore, the initially cylindrical beam contracted into a flat slab.

Once this behavior was observed, Lindberg demonstrated that the reverse deflection could be qualitatively understood on the basis on classical and electric circuit theory if the backward drift of high energy electrons were accounted for [Alfvén 1981]. When the plasma enters the curved field, it induces a transverse electric field $\mathbf{E} = -\mathbf{v} \times \mathbf{B}$. This region then becomes a generator driving the current in an upward, transverse, third dimension, that then becomes polarized because of its low transverse conductivity (Figure 7).

6. Further Developments in Plasma Simulation

6.1. Parallelism

As pointed out, data management problems dominate the subject of 3D plasma simulation using particles-in-cell. In the novel computer architectures, with their high degree of parallelism, data transport becomes an even more important issue. Computing efficiency depends critically on (topological or physical) data proximity in the basic procedure of a problem. "Local" algorithms, such as finite-difference equations, have preference over "global" algorithms, such as Fourier transforms (Note that the calculation of each single Fourier harmonic requires the entire data-base). With this in mind, new 3D plasma codes have been constructed. In these the particles are advanced just as in Eqs.(8.6)-(8.8), but Maxwell's equations are integrated locally over a cubic mesh in the form:

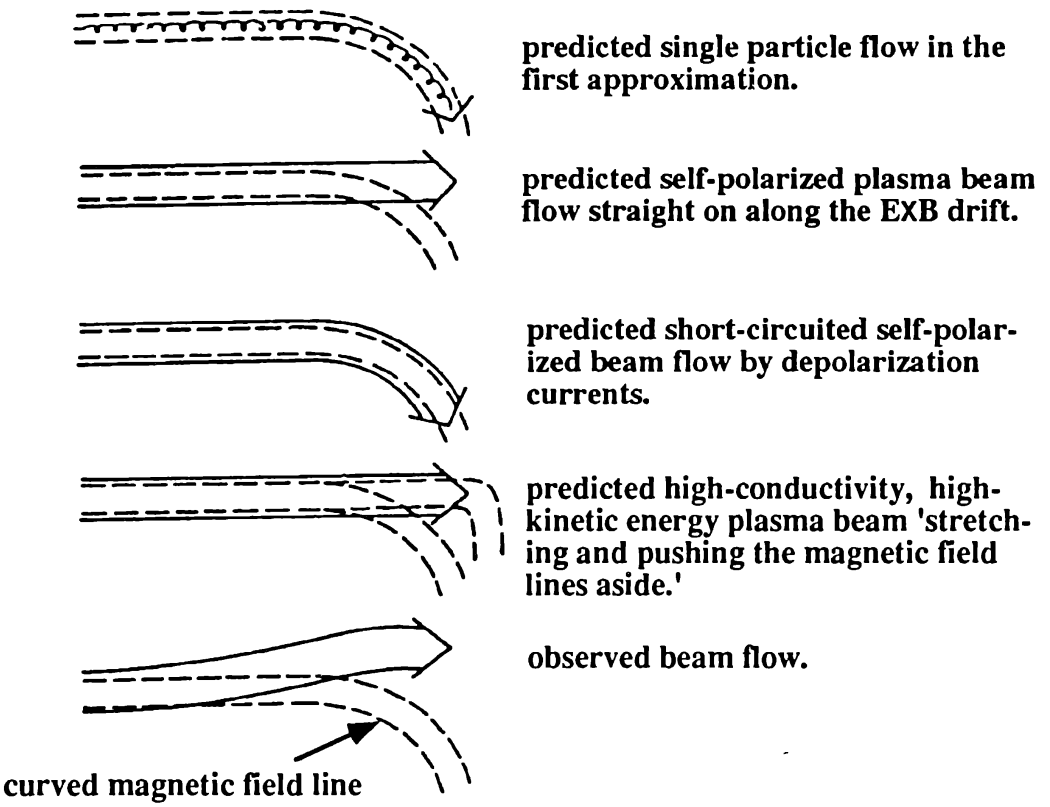

Figure 6. Classical predictions and the real behavior of a plasma beam, initially moving parallel to a guide magnetic field, when entering a curved field region. The last frame shows, contrary to all predictions, a reverse deflection of the beam out of the guide field. Only when the experiment is simulated in three dimensions is the correct solution, including beam flattening, obtained. Figure courtesy of H. Alfvén.

1. change of **B**-flux through a cell-face = - circulation of **E** around it.
2. change of **D**-flux through a cell-face = circulation of **H** around it - charge flow through it.

The **E**− or **D**− data mesh is staggered relative to the **B**− or **H**− data mesh both in space and time.

This method has the advantage that needs to be satisfied only at the beginning of a run (where it becomes a triviality of initialization): it is automatically carried forward in time by consistent determination of the charge flow between cells. Thus Poisson's equation does not have to be solved. Poisson's equation is "global": The solution anywhere depends on the data everywhere.

The algorithms for a simplified version of TRISTAN, a fully three-dimensional, fully electromagnetic, and relativistic PIC code, are found in *Physics of the Plasma Universe* [Peratt 1992].

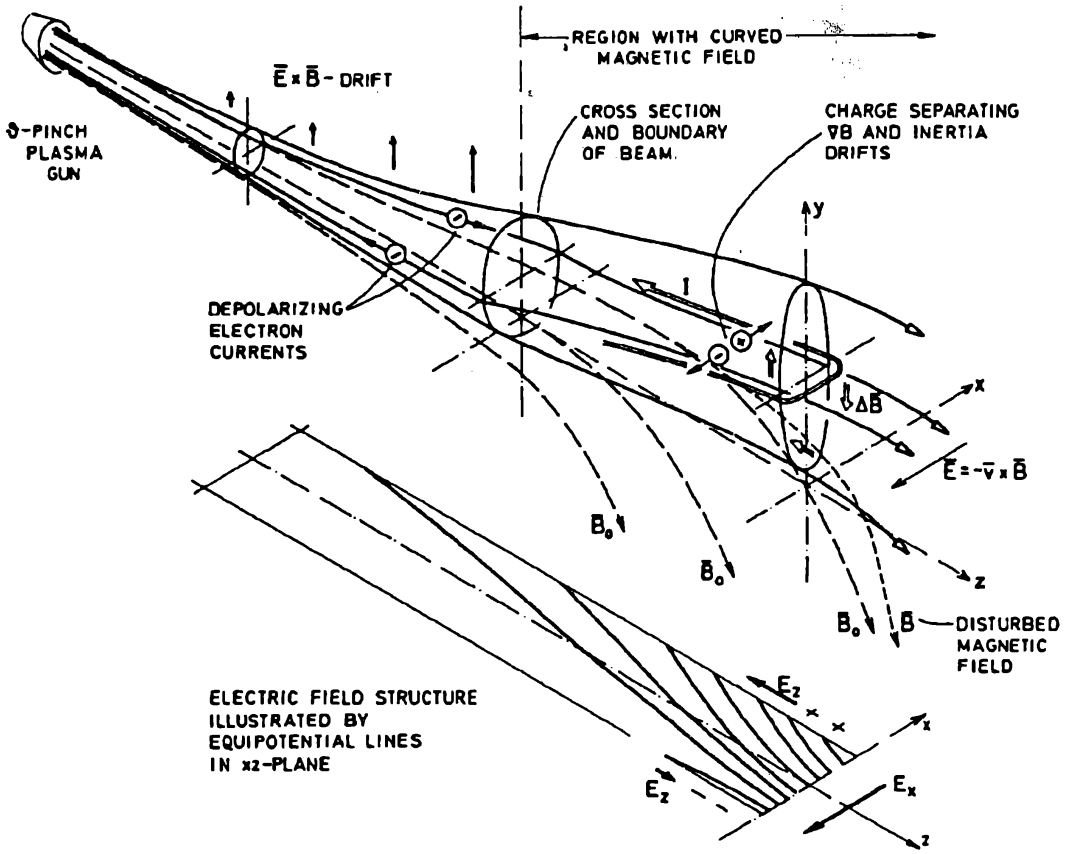

Figure 7. Kinetic and Electromagnetic components in the *Reverse Deflection Experiment.* Figure courtesy of H. Alfvén.

6.2. ISIS

ISIS is a multidimensional electromagnetic particle code, including three-dimensional capability, developed to treat particle-beam propagation in vacuum or plasma for realistic problems in pulsed-power transmission lines, high-power microwave generators, particle accelerators, and high-energy-density plasma applications. A description of the ISIS algorithms are given elsewhere [Jones and Peter 1985].

A major difference between ISIS and the older Fourier Transform versions of SPLASH or TRISTAN is that the ISIS uses finite-difference equations that are integrated over a spatial mesh having great generality in shape and coordinate system; e.g., the meshing may be nonlinear with many more zones inserted where known complex plasma motion occurs. Another major difference between SPLASH and ISIS is that in the former all quantities are scaled to the Debye length λ_D whereas in the latter all quantities are scaled to the Electromagnetic Skin Depth λ_E. In addition, affordable simulation with SPLASH/TRISTAN

is usually accomplished by using 'light ions.' A hybrid version of ISIS overcomes this problem.

All space-time relationships in ISIS are in cgs units[19]. Variables are scaled by a plasma frequency, ω_p^0, or equivalently, by a plasma density n_p^0, which is arbitrary. Code units are denoted by a tilde and are related to real units via the expressions:

$$\tilde{t} = t\omega_p^0, \ time$$

$$\tilde{x} = x\omega_p^0/c, \ length$$

$$\tilde{v} = v/c, \ velocity$$

$$\tilde{\gamma} = \gamma mc^2, \ energy$$

$$\gamma\tilde{v} = \gamma vmc, \ momentum$$

$$\tilde{E} = E\left(4\pi n_p^0 mc^2\right)^{-1} = eE/mc\omega_p^0 = (\lambda_E/511)\, E_{kV/cm}, \ electric\, field$$

$$\tilde{B} = B\left(4\pi n_p^0 mc^2\right)^{-1} = eB/mc\omega_p^0 = \omega_c^0/\omega_p^0, \quad magnetic\, field$$

The value of ω_p^0 may be defined in either of the following two ways:

1. Choose ω_p^0 = constant such the electromagnetic skin depth $\lambda_E = c/\omega_p^0$ is equal to an easily recognizable unit.

2. Once one parameter is fixed in a simulation, all other parameters can be scaled to it. For example, allow ω_p^0 to remain arbitrary by setting the code density of one species in the simulation to unity. Then lengths, times, electromagnetic fields, currents, etc., are scale to any arbitrary value of n_p^0 for that species. The density value of the other species are set by the ration of their density specified in the calculation to n_p^0.

Selection of the values of cell sizes ΔX, ΔY, ΔZ, and step size ΔT (where $X, Y, Z \equiv x, y, z/\lambda_E$, and $T \equiv \omega_p^0 t$) are very important to insure that the simulations has sufficient spatial and time resolution to solve the physics of the problem. In practice the stability constraints of ΔT are more demanding than those imposed by resolution and will determine its value. Spatially, at least six cells are required to resolve

[19] the text of this paper is in MKS units

a wavelength in any direction. A more appropriate number is twelve cells.

6.2.1. *Electrons as a massless fluid*

A hybrid ISIS model exists where the ions are treated kinetically via the PIC methods described above while the electrons are treated as a massless fluid. Hybrid simulation methods are useful in modeling low frequency plasma phenomena. The basic idea is to treat the electrons as a fluid, usually neglecting the electron mass and to treat the ions by the particle-in-cell method. This method allows following the dynamics of the plasma on the ion time scale, i.e., the ion gyroperiod in a magnetized plasma. The particle-in-cell method essentially solves the collisionless Boltzmann equation for the ions, giving a more complete description on the phase space evolution than a hydrodynamic model. Some approximations have been made that attempt to model the electron-ion collisional interaction, and ion-ion collisions have been treated through particle-pairing methods. As a result, hybrid methods, although suitable for following the time scales of interest, have not been optimally applied to high density collisional plasmas.

In general, the momentum equation for the electron fluid is

$$\begin{aligned} m_e\left(\tfrac{\partial v_e}{\partial t} + v_e \cdot \nabla v_e\right) &= -e\left(E + v_e \times B\right) \\ -\tfrac{\nabla(n_e k T_e)}{n_e} &- m_e \sum_i \nu_{ie}\left(v_e - v_i\right) \end{aligned} \tag{117}$$

where v_e and v_i are the electron and ion fluid velocities and ν_{ie} is the electron-ion collision rate. In taking the limit of this equation as m_e vanishes, it is assumed that ν_{ie} becomes infinite so that the product $\nu_{ie} m_e$ remains finite. Furthermore, we will assume quasineutrality, which allows us to replace n_e with $\sum_i Z_i n_i$, the ion density.

Taking the limit as m_e goes to zero and using the quasi-neutral assumption, we obtain

$$E = \frac{-j_e \times B}{\rho_e} - \frac{\nabla\left(\rho_e k T_e\right)}{\rho_e e} - \frac{m_e}{e}\sum_i \nu_{ie}\left(v_e - v_i\right) \tag{118}$$

where the ion charge density $\rho_i = -\rho_e = e n_e$ and j_e is the electron current density. In the usual hybrid approximation, this equation is solved for E under the assumption of a zero displacement current. The magnetic field is then advanced in time by Faraday's law Eq. 1.

The first term on the right hand side of Eq. 118 is used separately to advance the magnetic field in a subcycling procedure. The electron current density in this equation is determined from Ampère's law neglecting the displacement current and is given by

$$\mathbf{j}_e = \nabla \times \mathbf{B} - \mathbf{j}_i$$

In vacuum regions, the electric field is advanced with Ampère's law Eq. 2, including the displacement current. These equations are subcycled to satisfy the vacuum Courant condition. After the subcycling is completed, the last two terms of Equation 118 are added to the electric field and the corresponding magnetic field from Eq. 1 is also included. Using these electric and magnetic fields, the ions are treated in the usual particle-in-cell manner.

The second term of Equation 118 is the gradient of the electron pressure and is the usual hydrodynamic force term. The last term of Equation 118 is due to the collisional drag.

The electron temperature T_e in Eq. 118 can be entered via a number of different ways. For example, the simplest model would have only isothermal electrons. However, in general, the electron temperature would derive from an electron energy equation that includes electron-ion temperature coupling, electron-radiation coupling, heat transport, advection, and other electron energy source/sink mechanisms.

7. Advances in Numerical Modeling Techniques

7.1. Multi-Level Concurrent Simulation

The numerical modeling of complex physical phenomena requires the usage of a number of models of varying complexity. The near-Earth ionosphere-magnetosphere coupling problems is a prime example. Parts of the system require only simple electrical circuit analysis, while parts require a full first-principles treatment in fully three dimensional space. Not every step of the modeling process requires the most sophisticated models. In the past, it has been the modeler's responsibility to make intelligent choices as to which model to use and then the modeler would rely on experience and insight to interface the results of one code as inputs to the next code. This painstaking process has evolved today into what is called Multi-Level Concurrent Simulation (MLCS) [Jones 1995].

As a paradigm, MLCS is a way of facilitating the design by interfacing the various components of the process. Recent advances in distributed computing naturally lend themselves to this structure, using various computational tools from a variety of platforms to concurrently model various levels of the problem. This concept involves various pieces of computer hardware networked to access program libraries,

empirical design curves and powerful first principles physics models through a common interface.

In spite of the fact that modelers of complex plasma phenomena have developed expertise in areas such as implicit numerical techniques, hybrid models, adaptive grid methods and multiple time scale perturbation methods, modelers are still often faced with inadequate tools because of disparate time and spatial scales. Advances in computing hardware promised by the Accelerated Scientific Computing Initiative (ASCI)[20] offer the hope that more first principles approaches can be applied to complex problems. However, the demand always exceeds the resources. Furthermore, many models are not stable enough to be used for the extremely long time scales needed to model some systems from first principles, even if the computing resources are available.[21] Thus, robustness in new modeling techniques must match the new capabilities in hardware performance.

7.2. The Hierarchy of Scaling

The need for multiple time and spatial scale modeling in science is ubiquitous. Often modeling of physical systems is essentially impossible because first principles physical models are too resource intensive to be used on the space and time scales needed to answer the pertinent question at hand. Even if massively parallel computers can, in the near future, reach the teraflop regime as promised, present day algorithms and models may not be numerically stable enough to be useful. Systematic methods of treating multiple scales would significantly impact the modeling of complex plasma processes of laboratory or astrophysical dimensions and numerous other scientific disciplines. A NASA space weather initiative has need for accurate plasma models that reflect both large scale and small scale phenomena.

The coupling of disparate spatial and/or temporal scales is at the heart of many scientific modeling efforts and indeed forms the core research in modeling the effects of microphysics on macrophysics scales, including the effects of turbulence on hydrodynamic modeling, hybrid plasma simulation models for magnetic fusion and space plasmas, and subgrid models in electromagnetic modeling. Advanced modeling also has a need for physics of radiation transport, hydrodynamics, plasma physics, and atomic physics in integrated modeling tools. Most plasma

[20] ASCI is a U.S. Department of Energy program to advance the state of numerical computation by accelerating the current multi-hundred-megaflop, large platform, computer speed to the 100 teraflop (10^{14} floating operations per second), by the year 2002.

[21] In some circumstances involving multitasking applications on a Cray-YMP, where 6 processors are used simultaneously, 350 Mflops speeds can be reached.

physics problems exhibit an extended range of time and spatial scales. In particular space plasmas have multiple scales involving electron and ion motion, sheaths, and other phenomena that may involve the growth of instabilities, the generation of large electric fields, and the subsequent acceleration of the charged particles to high energies.

The difficulty in using existing tools concurrently is that there often exists a disparity in scale between the various models. Distributed computing is only part of the solution to this problem. Execution times for different models could be tailored to specific hardware on the network. For example, simple systems models may run concurrently on a personal computers while sophisticated physics models are running on the ASCI machines, filling in the unknown parts of the system database. Obviously one is not always lucky enough to have the answers come out at the right time to make this process efficient [Jones 1995].

Optimization of fidelity in physical modeling is paramount in the development of high-performance computing techniques. Multi-level concurrent computing now appears possible because of recent advances in numerical differencing techniques, and the availability of distributed computing resources. However, to make Multi-level concurrent simulation viable, development is required with regards to reduced space and time scales modeling, robust algorithms, distributed computing, and modular code construction.

7.3. Reduced Space and Time Scales

The basic problem is how to represent the fundamental, relatively small-scale, physical processes, which often take place at relatively small or microscopic length scales, in models which describe the relatively large or macro scale response of systems of interest with larger dimensions. Multiple time/spatial scale perturbation theory and other techniques may be used to formulate the effects of micro scale physics on longer space and time scales.

An example is the recent development of "collision field" methods to incorporate Coulomb collisions into a hybrid particle-in-cell code in order to model semicollisional plasmas. The effect of short range collisions is mediated through a field to study the nonfluid behavior of plasma in which the ion mean free path is comparable to the dimensions of the system being studied [Jones et.al. 1996]. This technique has been applied to ICF and magnetospheric problems [Jones et. al. 1995; Miller et. al. 1995].

7.4. Robust Algorithms

An example of robust algorithms is the work on coupling lumped circuit models to 3D Maxwell equation solvers. In this example, the disparate time scales make the problem numerically stiff. A complex form of time differencing involving multiple time scale analysis to integrate over the fast time scale to provide difference equations for the slower time scale proved to be a remarkably robust algorithm [Thomas et. al. 1994].

7.5. Distributed Computing

The subject of Multi-Level Concurrent Simulation (MLCS) is closely related to distributed computing, object oriented computing, and aspects of distributed computing that are gaining use such as object request brokers. The purpose of distributed computing is to couple models together. However a problem exists in distributed computing in that there are no accepted, platform independent methods presently for this type of approach to computing, and also the networks are rather slow as well. This problem may be solved in the marketplace in the next few years. A problem regarding the necessity of high data rate transfers apparently will be solved with introduction of optical networks leading to 38–42 GHz 'broadcast' transmitters at central locations with transceiver/antenna cards located on site.

The reason why the multi-processing client-server paradigm and object oriented programming fit well together is that the two deal with very different aspects of software. Whereas object oriented programming deals with abstractions of state and behavior, multiple processing deals with abstractions of schedule and sequence. These abstractions have very little overlap, so the two paradigms work well together.

7.6. Modular Code Design

The advantage of linking models together over multiple scales suggests a modular code development approach that adapts itself well to a hierarchy of space and astrophysical plasmas.

One can then envision modularizing the 3D full physics codes by using the MLCS approach to link independently developed modules for magnetohydrodynamics, transition regions, double layers, particle dynamics, and electromagnetic radiation.

8. Advances in Numerical Modeling Platforms

The necessity for ever faster and larger memory and storage capabilities in the computing environment is illustrated by the following example

involving the PIC simulation of an inertially confined plasma. Consider as the driver a neodymium glass laser beam at wavelength $\lambda_0 = 0.35\mu$m in the form of a pulse lasting several hundred picoseconds interacting with a cryogenic deuterium–tritium pellet with a total interaction volume of 1 mm^3. At this wavelength, the scale size of the simulation is approximately $3 \times 10^{10}\lambda_0^3$. For a mesh size of $\lambda_0/20$, this problem requires 2×10^{14} zones to simulate the laser-plasma evolution.

The field memory associated with this problem is ten or more words per zone[22]. The particle memory associated with this problem is six words per particle. Plasma spatial resolution requires about 100 particles per zone while 3 to 25 μs may be required to advance one particle per timestep in three dimensions. Particles dominate both memory and time. The particles require 600 words per zone and up to 2.5 ms per zone per timestep. Thus, this problem may require a total of 2×10^{16} particles, 1.2×10^{17} words (one cpu), and some 5×10^{11} seconds per timestep, i.e., sixteen thousand years.

Thus, the simulation of this problem appears intractable and when this analysis is applied to galactic dimensioned plasmas (of order 10^{65} particles), PIC simulation appears impossible.

However, postulate a computer capability of one central processor unit (cpu) per 60 megawords. This corresponds to ten million particles or a maximum of 250 seconds per timestep. For a one picosecond simulation, the timestep at the laser frequency $f = c/\lambda_0 = 8.96 \times 10^{14}$ Hz is approximately 1 ps/8.96×10^{14}Hz, or 4×10^6 cpu seconds (46 days).

Current three-dimensional PIC simulations generally employ 10-50 million particles, but as many as 250 million particles have been used. Expenditures of 350 cpu hours on an 8–processor, 32 Megaword, YMP machine to simulate a 3 million particle, 1 million cell plasma problem are not uncommon. However, to double the resolution of a PIC simulation requires a performance increase of 2^4, a factor 2 in each dimension plus a 1/2 timescale due to the Courant condition.

For a problem involving only a few hundred timesteps, a 3D PIC simulation on a Cray J90 dimensioned as $128 \times 128 \times 200$, with 206 megawords of memory might require 1.3×10^3 seconds (1.5 days) cpu time. If the dimensionality is increased by a factor $16 \times 16 \times 5$, the memory is increased to 264 gigawords and the time to 164×10^6 seconds (1900 days). For a dimensionality increase of $16 \times 16 \times 25$, the memory is 1.32 terawords and the time is 822×10^6 seconds (9500 days).

The increase in performance demand is also true of MHD codes. A 2D MHD code with 45×100 zones can require 9 hours cpu time on a YMP for problem completion. The addition of a third dimension

[22] This requirement depends on whether 32 bit words are used on a workstation or 64 bit (8 byte) words are used on a supercomputer.

Table I. Cray J90 hardware parameters.

Item	Parameter
Technology (CPU)	CMOS
Clock period	10 ns
Number of CPUs	32
CPUs per processor module	4
Peak performance	200 MFLOPS per CPU
Technology (memory)	70 ns CMOS DRAM
Memory size	1 - 8 Gbytes, (128 - 1024 Mwords)
Total memory bandwidth	51.2 Gbytes/s
Number of IOSs	16
I/O bandwidth	1.6 Gbytes/s

$45 \times 100 \times 100$ costs 100 times more and the inclusion of full radiation analysis takes 50 times as much time as the magnetohydrodynamics, so that 2000 equivalent YMP days are required. For convenience, typical operational parameters of a Cray J90 machine are tabulated in Table I.

However, these problems can be solved in about a day on a teraflop machine and in minutes on a petaflop machine.[23] Figure 8 illustrates the history of the performance speed of supercomputers and microprocessors versus year of operation.

In the United States, five governmental agencies are sponsoring the Petaflops initiative, the advancement of high performance computing capabilities into the petaflop (10^{15} flop) range. For example, the Department of Energy has established an Accelerated Strategic Computing Initiative (ASCI) whose purpose is to advance the availability of tightly coupled massively parallel processor and coupled shared memory processor clusters; and incorporating high-speed interconnects in a seamless, distributed computing environment. To achieve this goal, ASCI is supporting three memory options for the development of teraflop machines, respectively designated 'red', 'blue Pacific', and 'blue mountain'.

8.1. *ASCI Red*

The ASCI Red platform effort will bridge the gap between giga-scale and tera-scale computing to accommodate the five-order-of-magnitude increase in performance required by "full-physics", "full-system" sim-

[23] 1 Teraflop is equivalent to 5,455 YMP equivalents while a Petaflop is equivalent to 5 and one-half million YMP equivalents.

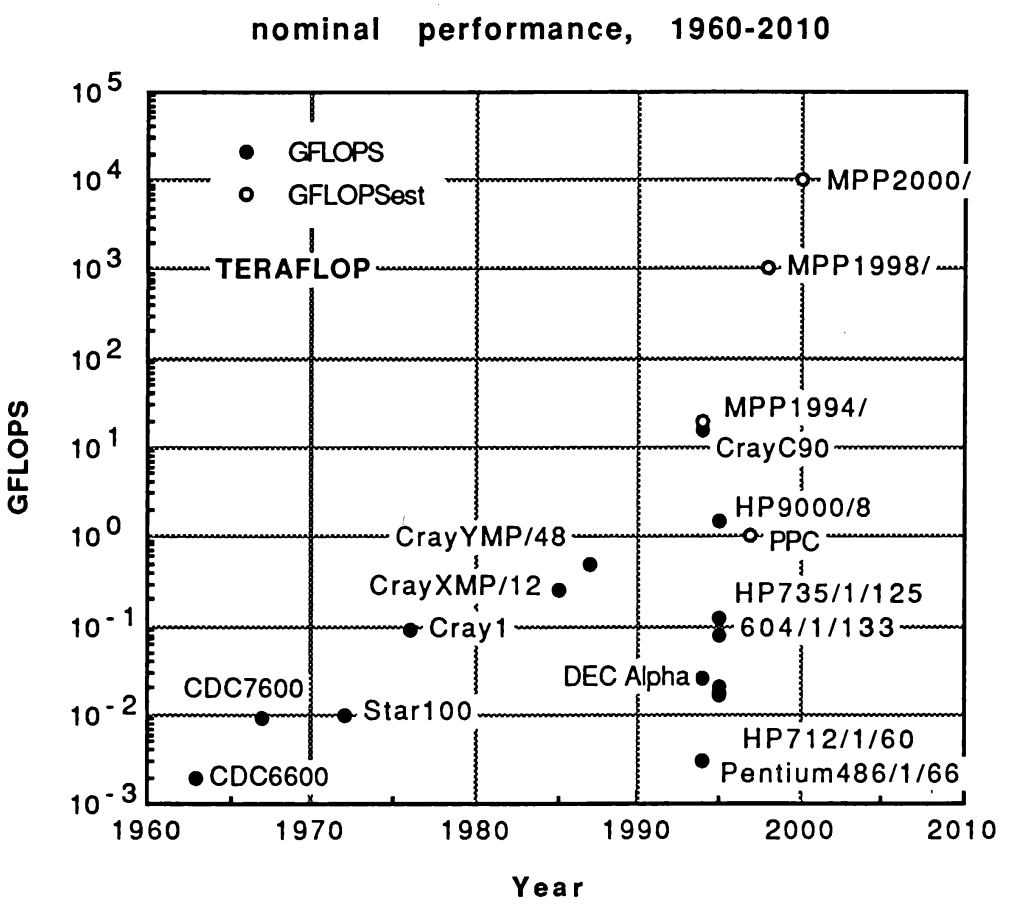

Figure 8. Performance speed of supercomputers and microprocessors versus year of operation.

ulation. The first deliverable in this effort is the 1.8 TFLOPS ASCI Red Supercomputer, a distributed memory system utilizing 9000 Intel P6 microprocessors and is nominally rated at 1.8 teraflops (1.8×10^{12}) flops with 512 gigabytes of memory (Figure 9). The machine will be located at Sandia National Laboratories.

8.2. *ASCI Blue Pacific*

A second platform called ASCI 'blue' is a shared memory processor system that consists of 512 nodes, each composed of eight-processor SMP units, for a total of 4096 IBM-Motorola PowerPC 604 RISC microprocessors. This machine has a rated capacity of 3×10^{12} flops and 2.5×10^{12} bytes of main memory. This machine is located at Lawrence Livermore National Laboratory.

Table II. ASCI Red system hardware parameters.

Item	Parameter
Compute Nodes	4,536
Service Nodes	32
Disk I/O Nodes	32
System Nodes (Boot and Node Station)	2
Network Nodes (Ethernet, ATM)	6
System RAM	594 MBytes
Topology	$38 \times 32 \times 2$
Node to Node bandwidth - Bi-directional	800 MBytes/sec
Bi-directional -Cross section Bandwidth	51.6 GBytes/sec
Total number of Pentium Pro Processors	9,216
Processor to Memory Bandwidth	533 Mbytes/sec
Compute Node Peak Performance	400 MFLOPS
System Peak Performance	1.8 TFLOPS
RAID I/O Bandwidth (per subsystem)	1.0 Gbytes/sec
RAID Storage (per subsystem)	1 TByte

Table III. ASCI Blue Pacific system hardware parameters.

Item	Parameter
Compute Nodes	512
Number of Microprocessors	4096
Microprocessors	PowerPC 604 (to be upgraded to to 630 chip)
RAM	64 MByte
Memory bandwidth	256 bit
Internal disk storage	2.2 Gbyte
Bus speed	160 MByte/sec
System Peak Performance	3 TFLOPS

8.3. *ASCI Blue Mountain*

A third machine, *ASCI Blue Mountain*, installed at Los Alamos National Laboraory is to have a nominal performance of three teraflops using 256 Silicion Graphics/Cray MIPS R10000(TM) microprocessors. A total of 3,072 processors will be in operation by 1999 providing a combined computational capability of 4 teraflops. The speed/memory delopment plan is outlined in Figures 9 and 10.

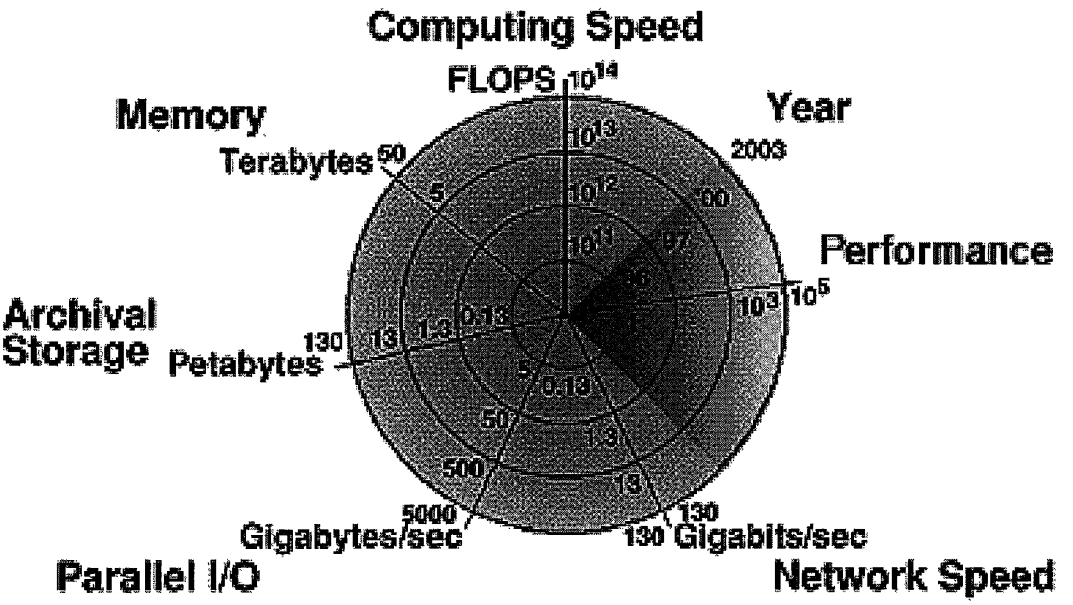

Figure 9. Estimated computing speed, memory, storage, transfer rates, and network speed versus year, 1996-2003.

9. Conclusions

Contrary to popular and scientific opinion of just a few decades ago, space is not an 'empty' void. It is actually filled with high energy particles, magnetic fields, and highly conducting plasma. The ability for plasmas to produce electric fields, either by instabilities brought about by plasma motion or the movement of magnetic fields, has popularized the term 'Electric Space' in recognition of the electric fields systematically discovered and measured in the solar system.[24] Today it is recognized that 99.999% of all observable matter in the universe is in the plasma state.[25]

[24] The metaphor 'Electric Space' was coined by Dr. Carolyn T. Brown, Assistant Associate Librarian for Area Studies (management of non-English collections and their scholarly use) at the Library of Congress and is the theme of the Space Science Institute traveling exhibition on the plasma universe supported by the National Oceanic and Atmospheric Administration and the National Science Foundation.

[25] The importance of electromagnetic forces on cosmic plasma cannot be overstated; even in neutral hydrogen regions ($\sim 10^{-4}$ parts ionized), the electromagnetic force to gravitational force ratio is 10^{7}.

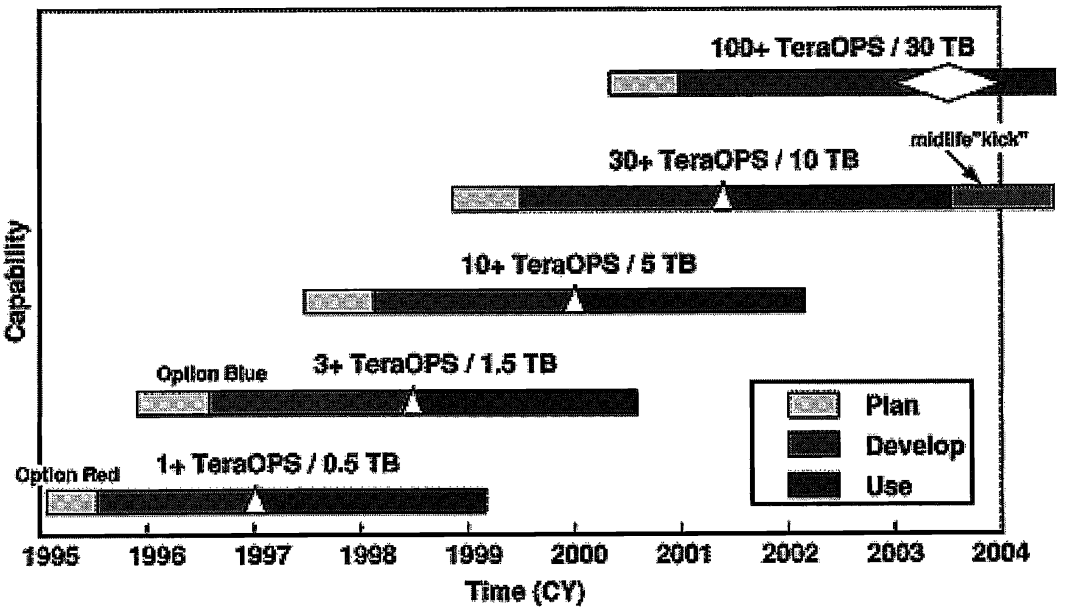

Figure 10. ASCI development and useage plan. Speed/memory in TeraOPS/Terabytes vs Calendar Year.

Plasma science is rich in distinguishable scales ranging from the atomic to the galactic to the meta-galactic. Plasmas of differing size or constituency also tend to be systematically coupled by electromagnetic forces. The problem of understanding the linkages and couplings in multi-scale processes is a frontier problem of modern science involving fields as diverse as high-energy-density plasmas in the laboratory to galactic dynamics.

Unlike the first three states of matter, plasma, the fourth state of matter, involves the mesoscale. Thus, in the study of astrophysical and space plasmas, the behavior of the near-earth plasma environment may depend to some extent on the solar and stellar plasmas that are part of the galactic plasmas. However, unlike laboratory plasmas, astrophysical plasmas will forever be inaccessible to in situ observation. The inability to test concepts and theories of large-scale plasmas leaves only virtual testing as a means to understand the universe. Advances in in computer technology and the capability of performing physics first principles, fully three-dimensional, particle–in–cell simulations, are mak-

ing virtual testing a viable alternative to verify our predictions about the far universe when the simulations are verified by benchmarking to high-energy-density plasmas produced in the laboratory by intense laser beam and pulsed-power facilities.

The advocacy of first principles numerical modeling of the plasma state requires the elimination of constructs or 'inventions' that were demanded by lesser capability machines used to support one and two-dimensional simulations. Thus, in synergism with availability of multi-teraflop computer platforms, particle-in-cell simulations devoid of the magnetohydrodynamic fluid approximations and in fully three-dimensional space are expected to find increasing application in modeling capabilities. The first principles approach will require a reexamination of the formulation used to describe the plasma state. The move from pure MHD to PIC simulation also makes possible the benchmarking of the radiation observed from either laboratory or astrophysical plasmas over the full electromagnetic spectrum, to the extent that the advanced platform will support the necessary space/temporal resolution.

To fully utilize the availability of sub-petaflop or petaflop computer speed/memory architectures, a new simulation methodology such as parallelism for multiprocessors and multi-level concurrent simulation techniques with its concomitant demands of the advancement in multiple time and spatial scaling, robust algorithms, distributed computing, and modular code design is required. The end benefit is sobering: simulations that today would require cpu times of decades will be completed in days and ultimately, minutes.

10. Acknowledgments

This work was performed under the auspices of the U.S. Department of Energy. The author thanks R. J. Barker, C. K. Birdsall, C.-G. Fälthammar, A. B. Langdon, and M. E. Jones for useful discussions.

References

Alfvén, H., Carlqvist, P.: 1978, *Astrophys. Space Sci.***Vol. no. 55**, 484

Alfvén, H., Herlofson, N.: 1950, *Phys. Rev.***Vol. no. 78**, 616

Alfvén, H. and Fälthammar, C.-G. : 1963, *Cosmical Electrodynamics*, Oxford University Press, New York

Akasofu, A.-I.: 1981, "Energy coupling between the solar wind and the magnetosphere", *Space Sci.Rev.***Vol. no. 28**, p.21

Bennett, W. H.: 1934, "Magnetically self-focusing streams", *Phys. Rev.***Vol. no. 45**, 890

Birdsall, C. K., Langdon, A. B. : 1985, *Plasma Physics via Computer Simulation*, McGraw-Hill, New York

Biskamp, D.: 1997, "Magnetic Reconnection in Plasmas", *Astrophys. Space Sci.,This issue*

Bogdankevich, L. S., Rukhadze, A. A.: 1971, "Sov. Phys. Usp", *Sov. Phys. Usp.***Vol. no. 14**, 163

Bostick, W. H.: 1986, "What laboratory produced plasma structures can contribute to the understanding of cosmic structures both large and small", *IEEE Trans. Plasma Sci.***Vol. no. 14**, 703

Brackbill, J.: 1987, "Fundamentals of Numerical Magnetohydrodynamics, International School for Space Simulation, La londe les Maures, France, 1987", *Los Alamos National Laboratory Report, LA-UR-87-2052.*

Buneman, O.: 1976, "The advance from 2D electrostatic to 3D electromagnetic particle simulations", *Computer Phys. Comm.***Vol. no.12**, pp. 21–31

Buneman, O., Barnes, C. W., Green, J. C., Nielsen, D. E.: 1980, "Principles and capabilities of 3D, EM particle simulations", *J. Comp. Phys.***Vol. no.38**, 1

Buneman, O.: 1986, "Multidimensional particle codes: their capabilities and limitations for modeling space and laboratory plasma", *IEEE Trans. Plasma Sci.***Vol.14**, 661

Carlqvist, P.: 1988, "Cosmic electric currents and the generalized Bennett Relation", *Astrophys. Space Sci.***Vol. no. 144**, 73

Chen, F. F. : 1984, *Introduction to Plasma Physics and Controlled Fusion*, Plenum Press, New York

Dawson, J. M., Decyk, V., Sydora, R., Liewer, P.: 1993, "High-performance computing and plasma physics", *Phys. Today.*, March

Eastman, T.: 1990, "Transition regions in solar system and astrophysical plasmas", *IEEE Trans. Plasma Sci.***Vol. no. 18**, p18.

Frank, I., Ginsburg, V.: 1945, "Radiation of a uniformly moving electron due it its transition from one medium into another", *Journal of Phys.***Vol. no. IX**, pp. 353–362

Gouveia Dal Pino, E. M., Opher, R.: 1989, "The origin of filaments in extended radio sources", *Astrophys. J.***Vol. no. 342**, pp. 686–699

Lindberg, L.: 1970, *Astrophys. Space Sci.***Vol. no. 55**, 203

Hammer, D. A., Rostocker, N.: 1970, *Phys. Fluids***Vol. no. 13**, 1831

Happek, U., Sievers, A. J., Blum, E. B.: 1992, "Observation of coherent transition radiation", *Phys. Rev. Lett*

Hockney, R. W., Eastwood, J. W.: 1981, *Computer Simulation Using Particles*, McGraw-Hill, New York

Jones, M. E., Peter, W. K.: 1985, *IEEE Trans. Nucl. Sci.***Vol. no. NS-32**, p. 1794.

Jones M. E. , D. S. Lemons, R. J. Mason, V. A. Thomas, & D. Winske: 1996, "A Grid-Based Coulomb Collision Model for PIC Codes", *J. Comput. Phys.***Vol. no. 123**, in press.

Jones, M. E., D. Winske, S. R. Goldman, R. A. Kopp, V. G. Rogatchev, S. A. Bel'kov, P. D. Gasparyan, G. V. Dolgoleva, N. V. Zhidkov, N. V. Ivanov, Yu. K Kochubej, G. F. Nasyrov, V. A. Pavlovskii, V. V. Smirnov, and Yu. A. Romanov: 1996, "An Adiabatic Fluid Electron Particle-in-Cell Code for Simulating Ion-Driven Parametric Instabilities", *Phys. Plasmas***Vol. no. 3**, pp. 1096-1108.

Jones, M. E.: 1995, "Multi-Level Concurrent Simulation: A White Paper", *unpublished*

Küppers, G., Salat, A., Wimmel, H. K.: 1973, "Macroscopic equilibria of relativistic electron beams in plasmas", *Plasma Phys.***Vol. no. 15**, 441

Melrose, D. B.: 1997, "Particle Acceleration and Nonthermal Radiation in Space Plasmas", *Astrophys. Space Sci.,This issue*

Miller, R. H., Combi, M. R.: 1995, *Geophys. Res. Lett.***Vol. no. 21**, 1735

Nahin, P. J. : 1988, *Oliver Heaviside: Sage in Solitude*, IEEE Press, New York

Peratt, A. L. : 1992, *Physics of the Plasma Universe*, Springer-Verlag, New York

Thomas, V.: 1995, "Multi-Level Concurrent Simulation", *Los Alamos National Laboratory Report LA-UR-95-3454*

Trubnikov, B. A.: 1958, "Plasma radiation in a magnetic field", *Sov. Phys. 'Dokladdy'***Vol. no. 3**, 136

Vu, H. X.: 1996, "An Adiabatic Fluid Electron Particle-in-Cell Code for Simulating Ion-Driven Parametric Instabilities", *J. Comput. Phys.***Vol. no. 123**, in press.

Witalis, E.: 1981, *Phys. Rev. A***Vol. no. 24**, 2758

Yonas, G., Poukey, J. W., Prestwich, K. R., Freeman, J. R., Toepfer, A. J., Clauser, J. J.: 1993, *Nucl. Fusion***Vol. no. 14**, 731

Zimmerman, G. B., Kruer, W. L.: 1975, *Comments Plasma Phys.***Vol. no. 2**, p. 51.